doi:10.1016/S0022-2836(02)00382-0 available online at http://www.idealibrary.com on IDEAL® J. Mol. Biol. (2002) 319, 1015–1034

JMB

Solution Conformations of Unmodified and $A_{37}N^6$-dimethylallyl Modified Anticodon Stem-loops of *Escherichia coli* $tRNA^{Phe}$

Javier Cabello-Villegas[1], Malcolm E. Winkler[2] and Edward P. Nikonowicz[1]*

[1]*Department of Biochemistry and Cell Biology Rice University, Houston TX 77251-1892, USA*

[2]*Department of Microbiology and Molecular Genetics University of Texas Houston Medical School, Houston TX 77030-1501, USA*

**Corresponding author*

The modification of RNA nucleotide bases, a fundamental process in all cells, alters the chemical and physical properties of RNA molecules and broadly impacts the physiological properties of cells. tRNA molecules are by far the most diverse-modified RNA species within cells, containing as a group >80% of the known 96 chemically unique nucleic acid modifications. The greatest varieties of modifications are located on residue 37 and play a role in ensuring fidelity and efficiency of protein synthesis. The enzyme dimethylallyl (Δ^2-isopentenyl) diphosphate:tRNA transferase catalyzes the addition of a dimethylallyl group to the exocyclic amine nitrogen (N6) of A_{37} in several tRNA species. Using a 17 residue oligoribonucleotide corresponding to the anticodon arm of *Escherichia coli* $tRNA^{Phe}$, we have investigated the structural and dynamic changes introduced by the dimethylallyl group. The unmodified RNA molecule adopts stem-loop conformation composed of seven base-pairs and a compact three nucleotide loop. This conformation is distinctly different from the U-turn motif that characterizes the anticodon arm in the X-ray crystal structure of the fully modified yeast $tRNA^{Phe}$. The adoption of the tri-nucleotide loop by the purine-rich unmodified $tRNA^{Phe}$ anticodon arm suggests that other anticodon sequences, especially those containing pyrimidine bases, also may favor a tri-loop conformation. Introduction of the dimethylallyl modification increases the mobility of nucleotides of the loop region but does not dramatically alter the RNA conformation. The dimethylallyl modification may enhance ribosome binding through multiple mechanisms including destabilization of the closed anticodon loop and stabilization of the codon–anticodon helix.

Keywords: prenylation; U-turn; RNA dynamics; translation defect; frameshift

Introduction

Post-transcriptional modification of RNA molecules occurs in all cells.[1–3] The modifications, which are primarily localized to the nucleotide bases, can alter the chemical, structural, and thermodynamic properties of RNAs and thereby contribute to RNA function. Nucleotide base modifications of RNA molecules

Present address: Malcolm E. Winkler, Infectious Diseases Research, Lilly Research Laboratories, DC 1543, Indianapolis, IN 46285, USA.

Abbreviations used: DMAPP, dimethylallyl diphosphate; $ACSL^{Phe}$, anticodon stem-loop of *E. coli* $tRNA^{Phe}$ (GAA); i^6A_{37} $ACSL^{Phe}$, A_{37} (N^6-dimethylallyl)-modified anticodon stem-loop of *E. coli* $tRNA^{Phe}$ (GAA); MiaA, dimethylallyl (Δ^2-isopentenyl) diphosphate:tRNA transferase; NTP, nucleoside triphosphate; NMR, nuclear magnetic resonance; NOE, nuclear Overhauser effect; NOESY, NOE spectroscopy; DQF-COSY, double quantum-filtered correlated spectroscopy; 2D, two-dimensional; 3D, three-dimensional; HetCor, heteronuclear correlation; HMQC, heteronuclear multiple quantum coherence; HSQC, heteronuclear single quantum coherence; MD, molecular dynamics; RMSD, root mean square deviation; NH, imino; NH_2, amino.

E-mail address of the corresponding author: edn@bioc.rice.edu

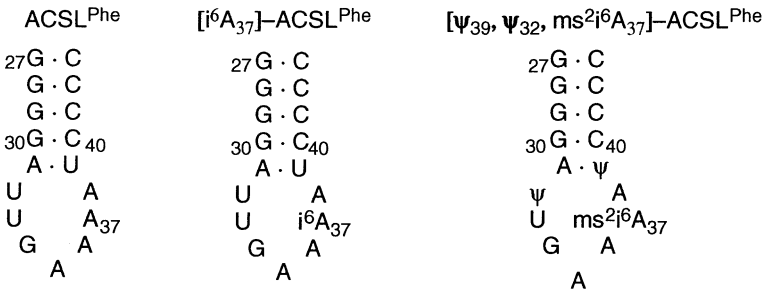

Figure 1. Sequences of the unmodified, i^6A_{37}-modified, and fully modified RNA hairpins corresponding to the anticodon arm of *E. coli* $tRNA^{Phe}_{GAA}$. Nucleotide numbering corresponds to the full-length tRNA molecule. ψ designates pseudouridine and ms^2i^6A designates (2-thiomethyl, N6-dimethylallyl)-adenine.

range from single methyl group additions, such as the conversion of guanosine to N7-methylguanosine, to complex multi-step, multi-enzyme reactions such as those leading to the production of (2-thiomethyl)-N6-dimethylallyl adenosine (ms^2i^6-adenosine). Many of the nucleotide base modifications have been chemically well characterized but the impact of these modifications on RNA structure and stability has been less thoroughly probed. Pseudouridine imparts thermodynamic stability to helices when located in the interior of an RNA duplex or in a single strand region adjacent to a duplex.[4] The ability of the pseudouridine base to form a hydrogen bond to the phosphate backbone may be key to its stabilizing property. The 5-methyl pyrimidines and 2-thiouridine also exhibit helix-stabilizing effects.[4,5] The methyl groups at the 5-positions of uridine and cytidine increase stability by enhancing base stacking. The C2 sulfur substitution of 2-thiouridine leads to a strong thermodynamic preference for the C3′-*endo* sugar conformation in the nucleoside.

tRNA molecules display the greatest diversity of modifications with more than 80 different types of modified nucleotides.[1,6] One of the most highly modified residues in tRNA is the nucleotide adjacent to the 3′ nucleotide of the anticodon, position 37.[7] In mature *Escherichia coli* $tRNA^{Phe}$, A_{37} is replaced by $ms^2i^6A_{37}$. The modification enzyme dimethylallyl (Δ^2-isopentenyl) diphosphate:tRNA transferase (MiaA) catalyzes the addition of the dimethylallyl unit from dimethylallyl diphosphate (DMAPP) to the exocyclic amino nitrogen (N6) of A_{37}, forming i^6A_{37}. This reaction, also referred to as prenylation, occurs at position 37 adenosines in ten of 46 *E. coli* tRNA species.[8–11] The enzymatic activities of MiaB and MiaC catalyze the methylthiolation of the i^6A_{37} intermediate to $ms^2i^6A_{37}$.

The $ms^2i^6A_{37}$ tRNA modification is important for normal cell function. *MiaA* mutants of *E. coli* and *Salmonella typhimurium* have many defects in translation, including decreased polypeptide chain elongation rates[12–14] decreased efficiency of translation[14] increased codon context sensitivity and decreased function of suppressor tRNA species that normally contain this modification[13–18] and decreased[15,16,18] or increased[19] translation misreading error rates at third or first positions in codons, respectively. The $ms^2i^6A_{37}$-associated defects lead to decreased growth rate and cell yield.[13]

Although several genetic studies designed to probe the physiological contribution of the A_{37} dimethylallyl modification have been conducted, the results have not been correlated with the structural consequences of this modification. The classic conformation of the anticodon arm of tRNA is based on the X-ray crystal structure of fully modified yeast $tRNA^{Phe}$.[20,21] The anticodon arm adopts a stem-loop motif composed of a five base-pair A-form helix capped by a seven nucleotide loop (Figure 1). The anticodon bases stack on the 3′-side of the loop with their Watson–Crick functional groups turned outward. A sharp turn between the highly conserved uridine at position 33 and the first anticodon nucleotide, position 34, is a characteristic structural feature of the loop and is designated the U-turn motif. The anticodon arm of the fully modified yeast and *E. coli* $tRNA^{Phe}$ species also has modified nucleotides at positions 32 and 39. Base modification at position 37 of tRNAs is believed to stabilize tRNA·mRNA interactions by improving intrastrand stacking within tRNA anticodon loops and interstrand stacking between codons and anticodons.[13,22] $ms^2i^6A_{37}$ is also believed to influence interstrand stacking interactions between wobble bases at position 34 in tRNA and bases immediately 3′ to codons,[7,13] although, direct structural evidence supporting these ideas is lacking.

We have used heteronuclear NMR spectroscopy to examine the solution structure and dynamics of the unmodified and MiaA-modified forms of the anticodon arm of *E. coli* $tRNA^{Phe}$. These studies were conducted using a 17 nucleotide RNA molecule that forms a stem-loop secondary structure in solution (Figure 1). Our results demonstrate that the loop of the unmodified RNA molecule is composed of three nucleotides and lacks the characteristic U-turn motif. Prenylation of the A_{37} base destabilizes the hairpin secondary structure near the loop and increases the dynamic properties of the loop and loop-proximal nucleotides. The fold of this purine-rich anticodon stem-loop suggests that anticodon arms with the potential to form a three-nucleotide loop will do so in the absence of appropriately positioned modifications. The altered structural and dynamic properties caused by dimethylallyl modification may facilitate codon–anticodon recognition by relaxing the closed and compact arrangement of nucleotide bases within the anticodon loop.

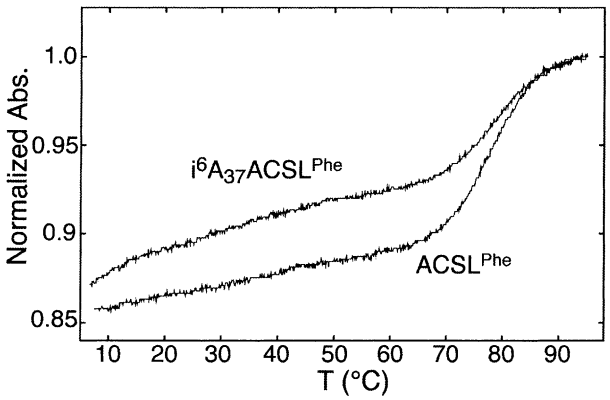

Figure 2. Overlay of the UV melting curves of the unmodified and i^6A_{37}-modified RNA hairpins. Each of the hairpins appears to exhibit two melting transitions—the broad lower temperature transitions presumably corresponding to destacking of the loop nucleotide bases. The apparent t_ms of the unmodified and i^6A_{37}-modified RNA hairpins are estimated to be 76.5 °C and 73.5 °C, respectively.

Results

Effect of dimethylallyl modification on RNA thermal stability

The thermal stability of the ACSL^{Phe} and i^6A_{37} ACSL^{Phe} RNA hairpins (Figure 1) was investigated using UV melting experiments to determine overall molecular stability (t_m). The UV thermal denaturation curves indicate that the hairpins melt in two stages (Figure 2). The lower temperature (<50 °C) transitions presumably correspond to the destacking of the loop nucleotides. The greater hyperchromicity of the i^6A_{37} ACSL^{Phe} molecule below 70 °C suggests that dimethylallyl modification decreases base stacking in the modified hairpin. The lack of increased thermal stability of the modified RNA hairpin is unexpected, since the dimethylallyl modification is predicted to enhance stacking of the anticodon bases.[13]

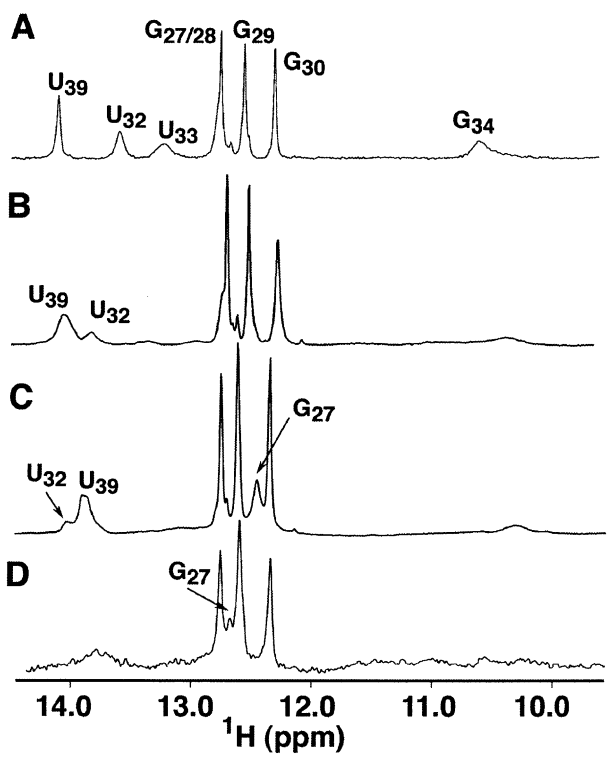

Figure 3. Imino ^{1}H spectra of (a) ACSL^{Phe}, (b) i^6A_{37}-modified ACSL^{Phe}, (c) ACSL^{Phe} in the presence of 7 mM Mg^{2+}, and (d) i^6A_{37}-modified ACSL^{Phe} in the presence of 7 mM Mg^{2+}. The sample for C was enzymatically dephosphorylated at the 5′-end.

The ACSL^{Phe} and i^6A_{37}ACSL^{Phe} molecules are hairpins in solution

Due to self-complementarity, the RNA sequence used in this study can form either a hairpin or a duplex with an internal loop. The structural features that distinguish these species, the loop of the hairpin and the internal loop of the duplex, may present similar nuclear Overhauser effect (NOE) patterns that could lead to misinterpretation of the NMR data. Indeed, experiments using non-denaturing polyacrylamide gel analysis suggest that the ACSL^{Phe} sequence forms a mixture of monomer and dimer species under buffer conditions similar to those employed for this investigation.[23] Each of the NH protons of the unmodified ACSL^{Phe} molecule gives rise to a peak in the one-dimensional (1D) NH ^{1}H spectrum (Figure 3(a)), but both hairpin and duplex species could yield this pattern. Thus, the oligomeric state of the RNA molecule was examined to confirm formation of the hairpin species. ^{15}N-labeled ACSL^{Phe} molecule was mixed with an equal amount of unlabeled ACSL^{Phe} variant molecule containing a $C_{42} \rightarrow U$ substitution. The $^{15}N-^1H$ heteronuclear multiple quantum coherence (HMQC) spectrum of the mixed sample in the presence and absence of Mg^{2+} contains the same G NH cross-peaks present in the spectrum of native ACSL^{Phe} RNA. No cross-peak corresponding to a G·U wobble base-pair is present in the spectrum of the RNA mixture. Since the ACSL^{Phe} variant molecules, which are not ^{15}N labeled, cannot give rise to cross-peaks in the HMQC spectrum, the G NH cross-peak of a G·U base-pair would only be observed if native and variant ACSL^{Phe} molecules formed heteromeric duplexes.[24] The analogous mixing experiments performed using ^{15}N-labeled i^6A_{37} ACSL^{Phe} yielded similar results and confirm the hairpin states of the ACSL^{Phe} and i^6A_{37} ACSL^{Phe} RNA oligonucleotides.

Resonance assignments of ACSL^{Phe}

The non-exchangeable ^{1}H and ^{13}C resonances of unmodified ACSL^{Phe} (Figure 1) were assigned using standard heteronuclear techniques.[25,26] The linewidths of the base and ribose 1′ ^{1}H resonances range between 3 and 4 Hz throughout the molecule. Most of the base and ribose $^1H-^{13}C$ correlations are resolved, and only the A_{37} H2

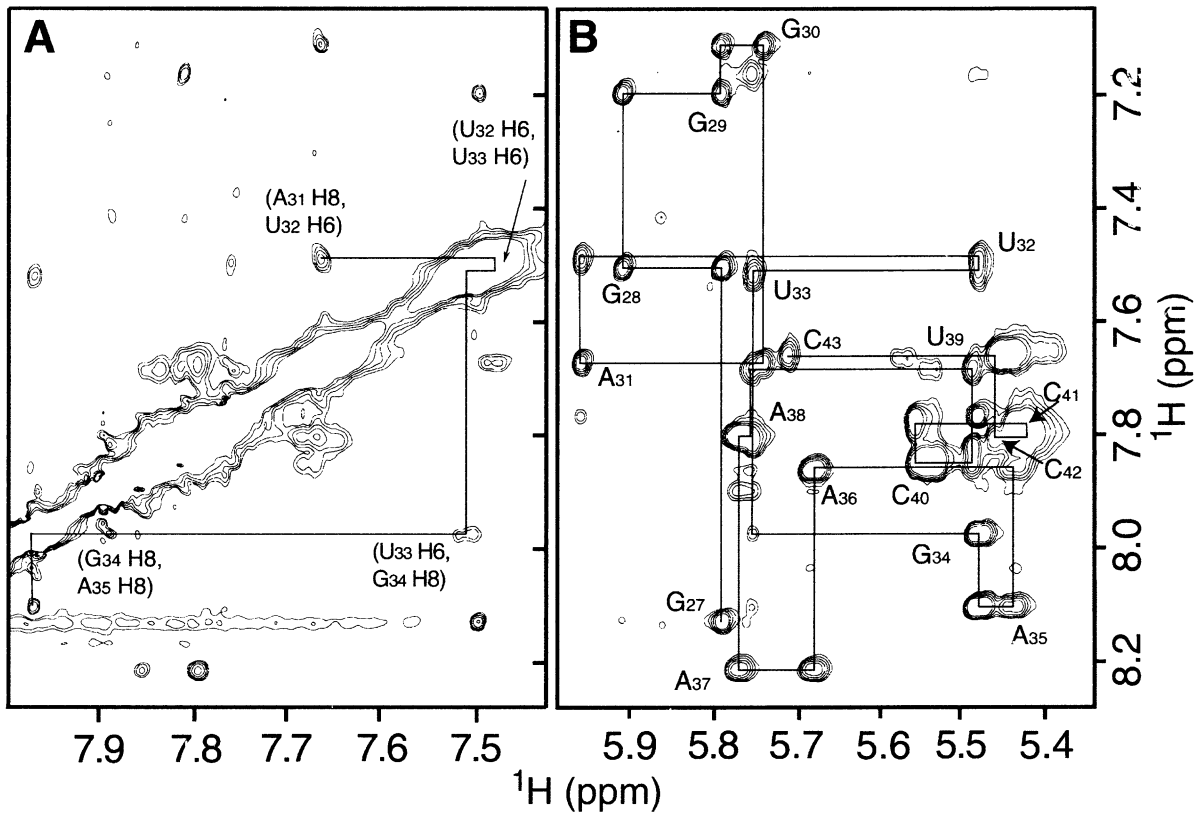

Figure 4. (a) Base H6/8-to-H6/8 and (b) H6/8-to-H1′ regions of the 2D 360 ms NOESY spectrum. The base-1′ proton sequential walk is traced with intra-residue peaks labeled. In (b), the arrows point to the inter-residue sequential NOE between U_{33} H1′ and G_{34} H8 and non-sequential NOE between U_{33} H1′ and A_{35} H8. The presence of the sequential NOE is not compatible with a U-turn motif for the loop whereas the non-sequential NOE can be produced by non-U-turn loop conformations. In (a), the sequential NOE between U_{33} H6 and G_{34} H8 is designated.

resonance has spectral characteristics indicative of intermediate exchange. All 17 ribose spin systems, except for the incompletely labeled 5′-terminal nucleotide, were identified using two-dimensional (2D) HCCH-COSY and three-dimensional (3D) HCCH-TOCSY experiments. The five adenine intra-base H8–H2 correlations also were identified using the HCCH-TOCSY experiment optimized for magnetization transfer through the adenine bases. Intra-residue base-to-sugar correlations were identified using 2D $^{15}N-^{1}H$ HSQC experiments optimized to yield the multiple bond correlations H5/6–N1, H8–N9, and H1′–N1/N9.[27] All purine correlations and five of seven pyrimidine correlations were identified in these spectra. Interestingly, H2′–N1/N9 correlations were observed for A_{31}, A_{35}, and C_{43}, suggesting these nucleotides do not have C3′-*endo* ribose ring puckers or that they have unusual transverse relaxation properties.

Sequential assignments for the non-exchangeable resonances were made using 2D NOE spectroscopy (NOESY) and 3D ^{13}C-edited NOESY experiments to identify sequential H6/8–H1′ NOE connectivities.[25] The intra-residue $^{15}N-^{1}H$ base-to-sugar correlations simplified the assignment process by permitting intra-residue cross-peaks to be distinguished from inter-residue cross-peaks. The sequential base-1′ NOE connectivities are continuous through all 17 nucleotides in the 180 ms NOESY spectrum (Figure 4), but the connectivity between nucleotides U_{33} and G_{34} is weak. The H6/8–H2′ and H6/8–H6/8 inter-residue connectivities also are continuous in the 180 ms spectrum except for the A_{35} H8 to A_{36} H8 step. Also, the base-2′ inter-residue connectivities from U_{32} to A_{37} are weak, consistent with the non-C3′-*endo* ribose ring conformations of these residues (described below). The sequential NOEs for the loop are summarized in Figure 5(a).

The exchangeable NH and NH_2 resonances were assigned using 2D NOESY experiments. Briefly, three strong G NH resonances corresponding to G·C base-pairs and three U NH resonances corresponding to A·U base-pairs were identified based on their characteristic ^{1}H and ^{15}N chemical shifts (Figure 3(a)). Three G NH and one U NH resonances were assigned using the NOE connectivities between NH proton resonances of adjacent base-pairs. These connectivities are continuous in the helix from G_{28} to U_{39}. The weak NH resonance of the terminal G·C base-pair does not yield cross-peaks in the NOESY spectrum. A weak G NH resonance, which has a chemical shift that corresponds to a non-base-paired guanine, was assigned to G_{34}. The U_{32} NH resonance was assigned from its NOE cross-peak with the A_{38} H2, since the U_{32}

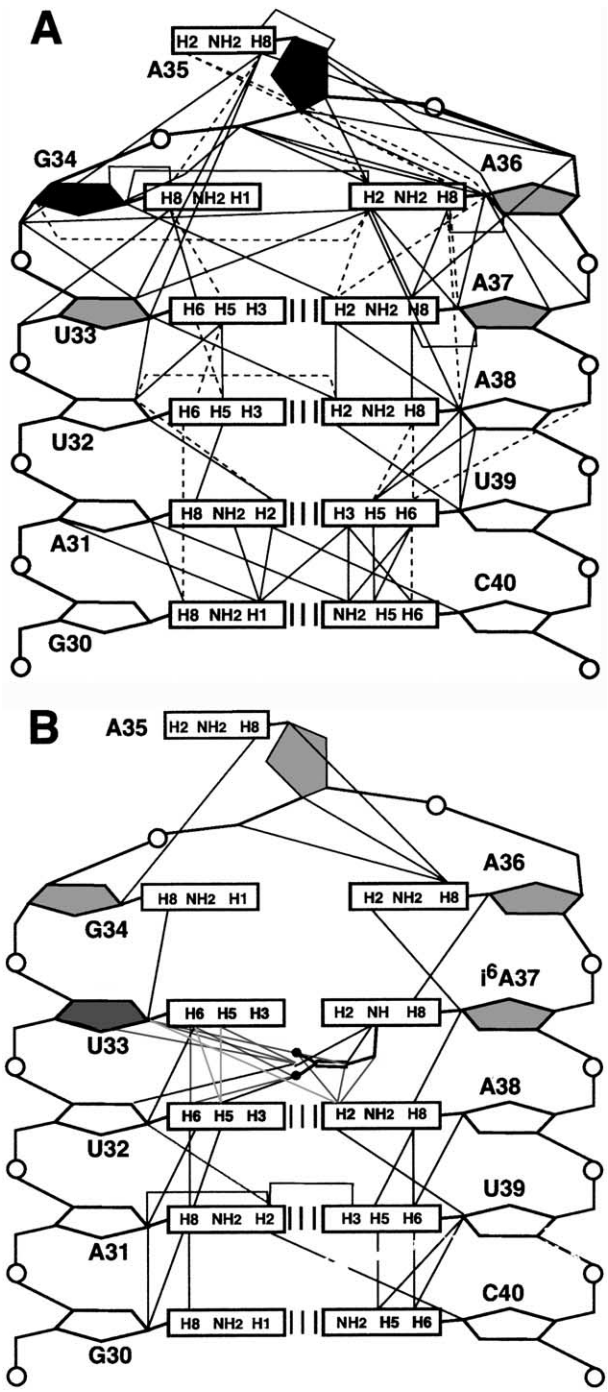

Figure 5. Schematic diagram summarizing several key NOEs identified in the loop regions of the (a) unmodified and (b) i^6A_{37}-modified RNA hairpins. Broken lines indicate NOEs identified only at experimental mixing times ≥180 ms and were assigned upper distance bounds of 7· to accommodate the possibility of spin diffusion. Ribose sugar conformations are indicated as C3′-*endo* (open), C2′-*endo* (filled), or mixed C3′/C2′-*endo* (gray).

H3 resonance is weak and does not give rise to a cross-peak with the U_{39} NH resonance. The U_{33} NH resonance is even weaker and could only be assigned through a U_{33} N3–A_{37} H2 cross-peak in a *J*(N, N)–HNN COSY spectrum (Figure 6).[28] The cytidine NH_2 resonances were assigned using the strong intra-base-pair C NH_2 to G NH NOE cross-peaks. Independent confirmation of the resonance assignments was provided by strong cytidine intra-base NH_2 to H5 NOE cross-peaks in G·C base-pairs and by uridine N3 to adenine H2 correlations in *J*(N, N)–HNN COSY spectra (Figure 6). The NH_2 resonances of A_{37} and A_{38} and of all guanine nucleotides except G_{34} were not observed. The A_{31} NH_2 resonances were assigned based on their NOE cross-peaks with U_{39} H3. The NH_2 proton resonances of A_{35} and A_{36} were assigned based on H2 to N6 correlations in the *J*(N, N)–HNN COSY spectrum. The NH_2 proton resonances of A_{35} and A_{36} are degenerate and have chemical shifts indicative of solvent-exposed protons.

All of the internucleotide phosphate ^{31}P resonances are clustered between −3.35 ppm and −4.63 ppm and were assigned using a ^{31}P–^{1}H hetero-TOCSY-NOESY experiment. The sequential P–H6/8 and P–H1′ correlations are continuous throughout the molecule. The P–H3′ correlations and several P–H4′ and P–H5′/H5″ correlations are present in ^{31}P–^{1}H HetCor spectra and provide independent confirmation of the ^{31}P assignments. The 5′-terminal phosphate resonates at −1.30 ppm and was assigned through cross-peaks to the ribose protons of G_{27}. Dephosphorylation of the RNA hairpin with alkaline phosphatase results in loss of the ^{31}P peak at −1.20 ppm and confirms its assignment as the terminal phosphate (Figure 7).

Resonance assignments of i^6A_{37} ACSL^{Phe}

The enzymatic prenylation of ACSL^{Phe} to i^6A_{37} ACSL^{Phe} was carried out on isotopically enriched RNA oligonucleotides, permitting the use of the same heteronuclear assignment strategies that were applied to unmodified ACSL^{Phe}. The dimethylallyl modification at A_{37} N6 broadens several of the base and 1′ resonances from U_{32} to A_{38} in ^{13}C–^{1}H correlated spectra and leads to absence of these 1′ resonances from the ct-HSQC spectrum. Nonetheless, all the 1′ and 2′ resonances except those of G_{34} and A_{35} were assigned using a combination of HCCH-COSY and NOESY spectra. The base 5 and 6 resonances of U_{33} and base 8 resonances of G_{34}, A_{36}, and A_{37} are broadened in the ^{13}C–^{1}H HMQC spectrum. Four of the five adenine H2 resonances can be observed in spectra of the modified ACSL^{Phe} and were assigned using the HCCH-TOCSY experiment. The H2 of A_{37} is not observed and presumably is broadened by chemical exchange.

The sequential assignment of the modified ACSL^{Phe} was complicated by broadening of loop nucleotide resonances. Resonance broadening from U_{32} to U_{39} leads to the loss of several intraresidue N1/9–H1′ correlations from the multiple bond ^{15}N–^{1}H HSQC spectrum as well as weakening of H6/8–H1′ correlations in NOESY spectra. G_{34} was assigned based on comparison of H8/C8 and ribose 2′ and 3′ chemical shifts of unmodified ACSL^{Phe} and a sequential H8–H1′ cross-peak with

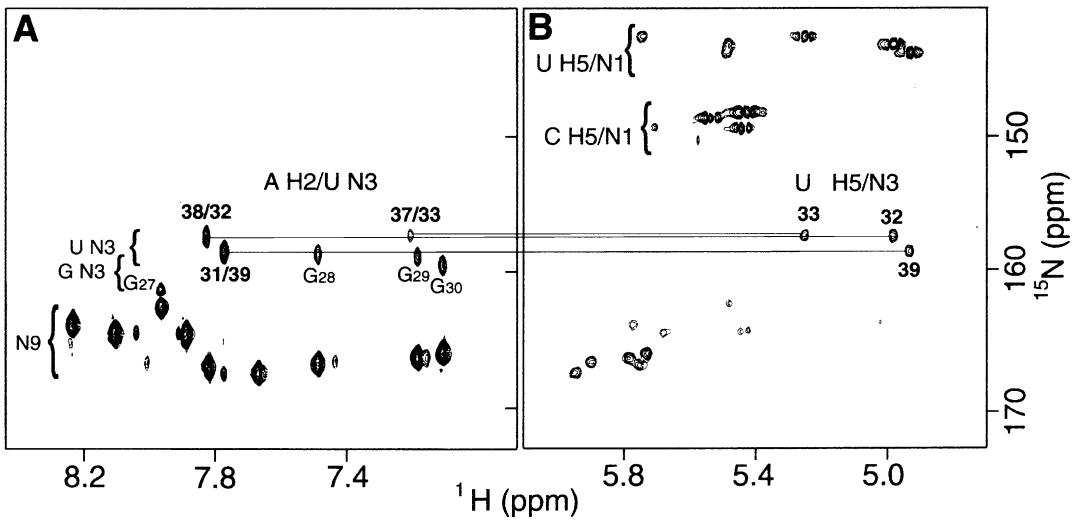

Figure 6. (a) Base proton to base nitrogen region of the *J*(N, N)–HNN COSY spectrum and (b) H5/H1′-to-base nitrogen region of the ^{15}N–^{1}H HSQC spectrum optimized multiple bond correlations. Horizontal lines connect the inter-base correlations between A_{31} H2 and U_{39} N3, A_{37} H2 and U_{33} N3, and A_{38} H2 and U_{32} N3 to the corresponding intra-base U H5–N3 correlations. Also contained in B are the two and three-bond intra-residue correlations between purine N9–H8/H1′ and pyrimidine N1–H5/H1′.

U_{33}. The G_{34} H1′ was assigned from the ^{31}P–^{1}H hetero-TOCSY-NOESY spectrum. The A_{35} H8 has no sequential NOEs but its chemical shift relative to $ACSL^{Phe}$ and the inter-residue correlation with the U_{33} H1′ are preserved. The A_{36} H8 resonance was identified through the sequential A_{35} H1′ cross-peak and conserved NOEs to A_{35} H4′ and H5′ resonances. The A_{37} H8 resonance remains the most downfield resonance, but intra- and inter-residue base-to-ribose cross-peaks are weak. The A_{38} H8 has an inter-residue cross-peak pattern typical for an A-form helical segment and includes interactions with U_{39} H5 and A_{37} H2′ resonances. The sequential NOEs for the loop are summarized in Figure 5(b).

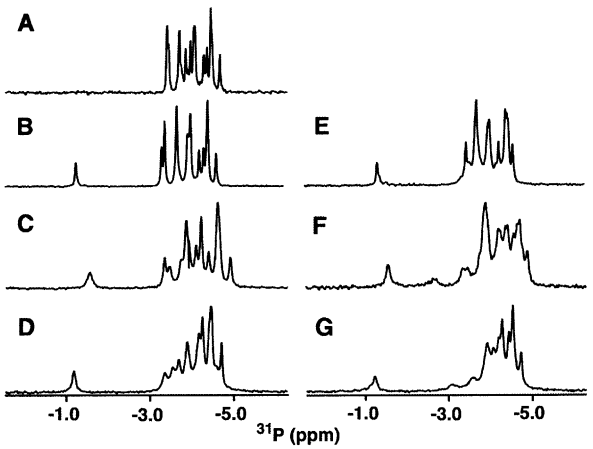

Figure 7. One-dimensional ^{31}P spectra of ((a)–(d)) unmodified and ((e)–(f)) i^6A_{37}-modified RNA hairpins without Mg^{2+} at 22 °C ((b) and (e)) and 5 °C ((c) and (f)) and with Mg^{2+} at 22 °C ((d) and (g)). Except for some broadening, the ^{31}P spectra are very similar indicating the RNA hairpin backbone conformation is not substantially altered by the A_{37} base modification or by the presence of Mg^{2+}. The ^{31}P spectrum of the phosphatase treated unmodified RNA hairpin (a) demonstrates that the ^{31}P resonance at −1.20 ppm corresponds to the 5′-terminal α phosphate. The ^{31}P resonances corresponding to internal bridging phosphate groups cluster between −3.3 ppm and −4.6 ppm, suggesting all α and ζ torsion angles have the standard *gauche*$^-$ conformation.

The exchangeable resonances of the RNA hairpin also are affected by the modification. The NH resonances of U_{33} and G_{34} are absent from the ^{15}N–^{1}H HMQC spectrum. The NH resonances of U_{32}, U_{39}, and G_{40} are broadened by the modification and appear less intense (Figure 3(b)). The NH_2 region is largely unchanged by the A_{37} modification with one exception. The A_{37} base now gives rise to a cross-peak corresponding to the N6 secondary amine (^{1}H = 6.71 ppm). The NOESY spectrum also contains cross-peaks involving this N6 proton resonance.

Like the unmodified RNA hairpin, the ^{31}P spectrum of the modified $ACSL^{Phe}$ does not contain any resonances that are shifted down field at either low or elevated temperatures (Figure 7). The chemical shifts corresponding to ^{31}P nuclei 5′ to G_{34}, A_{37}, and A_{38} are not conserved relative to those of the unmodified RNA hairpin and could not be unambiguously identified from the 1D spectrum. The chemical shift changes of these ^{31}P resonances may reflect conformational differences between the phosphate backbones of the two hairpins. However, no resonances are shifted dramatically down field that would be indicative of *trans* conformations for α and ζ in the i^6A_{37} $ACSL^{Phe}$ molecule.[29]

The ^{1}H resonances of the dimethylallyl group were assigned using NOESY spectra. The ^{1}H chemical shifts—CH, 6.78 ppm; CH_2, 3.76 ppm

Table 1. Summary of experimental distance and dihedral angle constraints and refinement statistics

Constraint	
NOE distance constraints	
Intra-residue[a]	101
Inter-residue	193
Mean number per residue	17
NOE constraints by category	
Very strong (0.0–3.0 Å)	7
Strong (0.0–4.0 Å)	24
Medium (0.0–5.0 Å)	69
Weak (0.0–6.0 Å)	108
Very weak (0.0–7.0 Å)	86
Base-pair constraints	
Total[b]	36
Dihedral angle constraints	
Ribose ring[c]	24
Backbone	46
Mean number per residue	4.1
Violations	
Average distance constraints >0.3 Å[d]	0
RMSDs for distance constraints (Å)	0.031
Average dihedral constraints >0.5°[e]	5.0
RMSDs for dihedral constraints (°)	0.28
RMSD from ideal geometry[f]	
Bonds (Å)	0.006
Angles (°)	1.369

[a] Only conformationally restrictive constraints are included.
[b] The number of base-pair constraints includes U_{33}·A_{37} base-pair constraints.
[c] Three torsion angles within each ribose ring were used to constrain the ring to either the C2′-*endo* or C3′-*endo* conformation. The ring pucker of residues U_{33} and A_{37} were not constrained.
[d] A distance violation of 0.3 Å corresponds to 5.0 kcal energy penalty.
[e] A dihedral angle violation of 0.5° corresponds to 0.05 kcal energy penalty.
[f] Calculated for the minimized average structure.

and 3.56 ppm; CH_3 1.56 ppm and 1.52 ppm—are similar to those reported for free dimethylallyl.[30] The proton linewidths of the dimethylallyl group range between 25 and 40 Hz and do not yield cross-peaks in the COSY spectrum. All protons of the dimethylallyl group have NOE cross-peaks to the N6 secondary amine proton of A_{37}. The dimethylallyl ^{13}C resonances were not assigned.

Structure calculations

The structure of ACSL^{Phe} was calculated using a restrained molecular dynamics routine starting from 60 sets of coordinates with randomized backbone dihedral angles. The calculations used a total of 294 distance constraints and 70 dihedral angle constraints (Table 1) to produce eight converged structures (Figure 8). Structures were classified as converged if they were consistent with the NMR data and maintained correct stereochemistry. The converged structures have an average of seven distance constraint violations between 0.1 Å and 0.3 Å, most of these involving the loop region. All converged structures have no constraints violated by more than 0.3 Å. When the structures are arranged in order of increasing overall energy, the converged structures form a plateau with similarly low overall energies and constraint violation energies.[31] The average root mean square deviations (RMSDs) of the heavy atoms between the individual structures and the minimized mean structure is 0.52 Å for the loop region (residues 32–38) and 1.57 Å for the stem region (residues 27–31 and 39–43). The unexpectedly large value for the stem originates from a bend in the helix axis between base-pairs G_{30}·C_{40} and A_{31}·U_{39} (Figure 9). This bend is not due to unusual NOEs or torsional angles but is consistent with observations from other studies[31] that NMR methods define the long-range structure of helical RNAs with less precision than they define local structure. The global fold of the unmodified ACSL^{Phe} is a hairpin composed of a seven base-pair stem and a three nucleotide loop (Figure 9). The overall fold of i^6A_{37} ACSL^{Phe} (a six base-pair stem with a five nucleotide loop) is similar to the unmodified hairpin, but the dynamics introduced by the modification lead to a less precisely defined loop conformation and loss of secondary structure proximal to the loop. Due to the sparseness of conformationally restrictive NOEs, a separate set of calculations was not performed using the modified RNA hairpin.

Structure of the loop region of ACSL^{Phe}

The loop of ACSL^{Phe} is composed of nucleotides G_{34}–A_{36} and is closed by the U_{33}·A_{37} base-pair (Figures 9 and 10(a)). The purine rings of G_{34} and A_{35} create a platform at the terminus of the hairpin. The base of G_{34} stacks against the base of U_{33}, consistent with the observed H6–H8 and H5–H8 NOEs. The bases of G_{34} and A_{35} are approximately coplanar and their C8–N1 vectors are parallel with each other. This orientation of the bases is consistent with a weak G_{34} H8–A_{35} H8 NOE cross-peak. The position of the A_{36} base is restricted by several NOEs involving its H2 resonance, including interactions with the H1′ resonances of G_{34}, A_{35}, A_{37}, and A_{38}, the H2′ of U_{33}, the H8 of A_{35}, and the H2 of A_{37} (Figure 5(a)). These NOEs position the base of A_{36} beneath the minor groove edge of the A_{37} base and between planes defined by the U_{33} and G_{34} bases (Figure 10(a)). The C8–N1 vector of A_{36} is anti-parallel with that of A_{35} but the configuration about the glycosidic bond is *anti*.

Several nucleotides in the loop have unusual sugar-phosphate backbone conformations. The large H1′–H2′ couplings of residues G_{34}–A_{36} indicate that their ribose sugar rings have the C2′-*endo* conformation. Residues U_{33} and A_{37} at the junction of the loop and stem have a mixture of C2′ and C3′-*endo* conformations as evidenced by their intermediate H1′–H2′ couplings and the modest downfield chemical shifts of their C3′ and C4′ resonances. The >5 Hz P–C2′ coupling

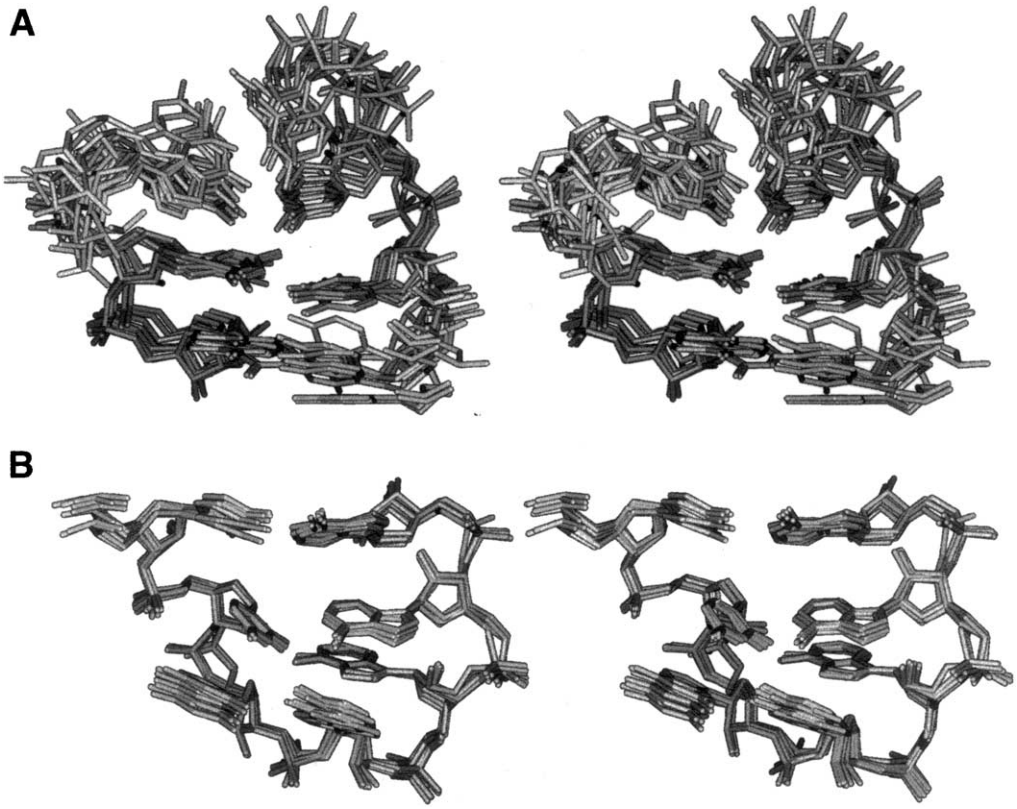

Figure 8. Stereo superposition of (a) the stem region (G_{28}–A_{31} and U_{39}–C_{42}) and (b) the loop region (U_{32}–A_{38}) from the ten lowest energy structures of the unmodified RNA hairpin. Only sugar and base heavy atoms are shown. Heavy atom RMSDs between the overlain structures and the average structure are 0.52 and 1.57 Å for the loop and stem regions, respectively.

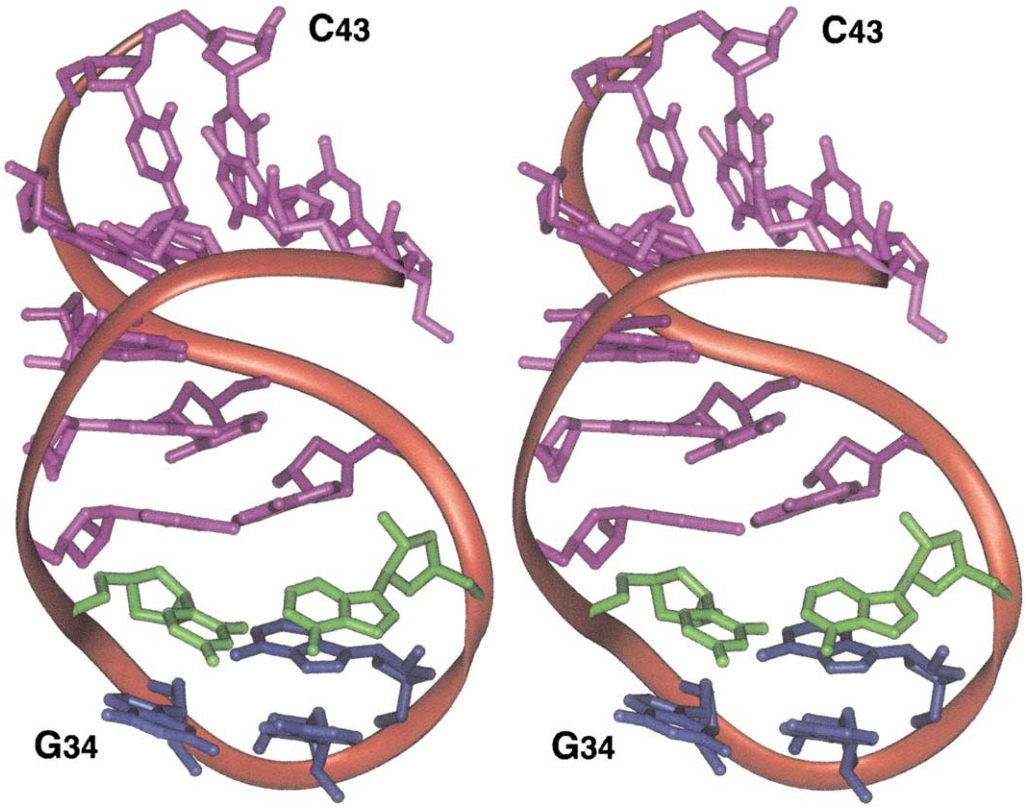

Figure 9. Stereoview into the major groove of the average minimized model of the unmodified ACSL^{Phe} RNA hairpin. The U_{33} and A_{37} nucleotides (green) form a Watson–Crick base-pair and stack above the anticodon bases (blue). No constraints were applied to enforce planarity of the U_{33}·A_{37} base-pair.

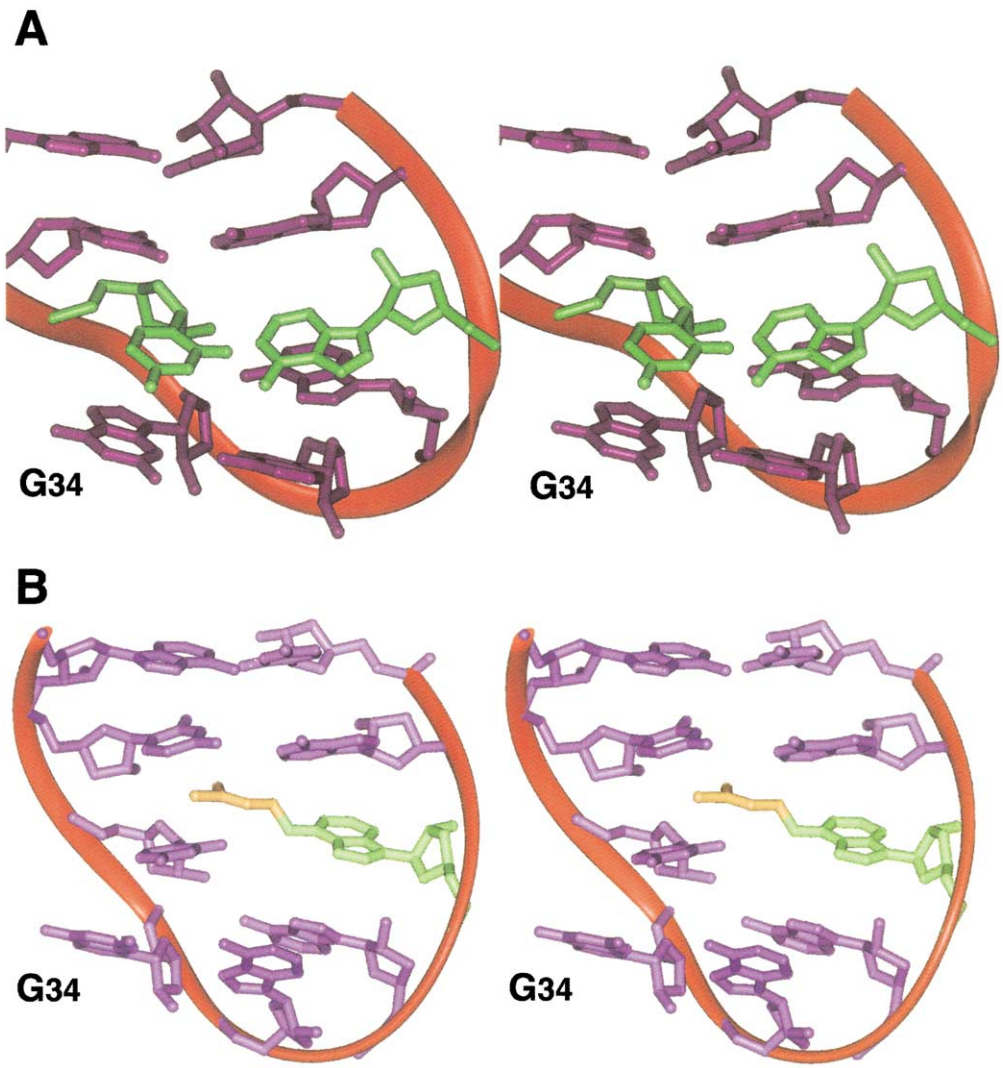

Figure 10. Stereoviews of the loop regions of (a) the unmodified and (b) the i^6A_{37}-modified RNA hairpins. The model of the i^6A_{37}-modified loop was created beginning with the structure of the unmodified loop. In (b), the dimethylallyl group (yellow) and the base of A_{37} (green) are recessed into the minor groove and the U_{33}·A_{37} base-pair is disrupted. Also, the positions of the G_{34} and A_{35} bases are less precisely determined in (b) due to resonance broadening.

for A_{35} indicates that its ε torsion angle has the non-standard *gauche*$^-$ conformation but the P–C2′ couplings of G_{34} and A_{36} indicate the corresponding ε angles are neither pure *gauche*$^-$ or *trans*. A_{36} has the largest error range of the C2′–P coupling constant among the loop nucleotides (≈4 Hz) and its ε torsion angle has the *gauche*$^-$ conformation not typical of A-form geometry. Therefore, only the *gauche*$^+$ conformation can be excluded for ε of residues G_{34} and A_{36}.

The *trans* conformation of either the α or ζ torsion angle is predicted to cause a 2–3 ppm downfield shift of the ^{31}P resonance. The ^{31}P resonances corresponding to the loop region form part of the main cluster of peaks between −3.35 ppm and −4.60 ppm, indicating that all α and ζ torsion angles probably occupy the *gauche* conformation. However, α and ζ were not constrained from U_{32}(p)U_{33} to A_{37}(p)A_{38} to allow for the possibility of conformational averaging. The ^{31}P spectrum at 5 °C also was examined to determine if a population of molecules is present that has an unusually structured but dynamic backbone conformation. However, no resonances with chemical shifts indicative of an unusual conformation are present (Figure 7).

A superposition of the loop regions from the eight converged structures is shown in Figure 8(b) and the minimized average structure is shown in Figures 9 and 10(a). The helical base stack is continuous along the 5′-side of the loop, with G_{34} stacking against the U_{33} base. On the 3′-side of the loop, the A_{37} base straddles the bases of A_{35} and A_{36}. The A_{36} N6 is 3 Å from the U_{33} O2′ in half of the converged structures, suggesting the possibility of a cross strand base–sugar hydrogen bond. However, this interaction could not be confirmed, since the A_{36} NH_2 proton resonances could not be assigned and no 2′-OH proton resonances were identified.

The loop of the $ACSL^{Phe}$ does not contain the classical "U-turn" motif. The presence of the inter-residue U_{33} H1′–G_{34} H8 and U_{33} H6–G_{34} H8 NOE cross-peaks is consistent with the relative U_{33} and G_{34} positions shown in Figure 10(a) but not with their positions in the U-turn. The ribose puckers of the anticodon nucleotides also tend towards the C3′-*endo* conformation rather than the C2′-*endo* conformation observed in this study. Another feature characteristic the U-turn motif is the *trans* conformation of backbone torsion angle α between U_{33} and G_{34}. The ^{31}P resonance corresponding to this phosphate is located in the main cluster of ^{31}P peaks (Figure 7). The chemical shift of this resonance is not consistent with the ^{31}P chemical shift predicted for a phosphate having the *trans* conformation of the α torsional angle.

However, to test the compatibility of the experimental NOE and coupling constant data with the backbone torsion angles characteristic of the U-turn motif, a second set of calculations was performed in which backbone torsion angles derived from the crystal structure of yeast $tRNA^{Phe}$ were used as constraints. Whether or not the U_{33}·A_{37} base-pair is constrained, residues 34–36 adopt the same configuration as the structures calculated without applying constraints for the torsional angles observed for the U-turn motif. However, the converged structures have higher overall energies than do structures not incorporating the U-turn specific torsional angle constraints and several of these constraints were violated. These structures also have more distance constraint violations, an average 8.5 violations >0.1 Å per structure. Thus, imposition of torsion angle constraints on the backbone alone is not sufficient to drive formation of the U-turn and they appear to be in opposition with some of the NOE-derived distant constraints.

Structure of the stem of $ACSL^{Phe}$

The geometry of the hairpin stem, base-pairs G_{27}·C_{43} to U_{33}·A_{37}, is primarily A-form (Figure 9). H6/8–H6/8 and H6/8–H1′,H2′ NOEs from 360 ms and 150 ms mixing time NOESY spectra, respectively, are continuous through this region of the RNA hairpin. The A_{31}·U_{39} and U_{32}·A_{38} base-pairs are sufficiently stable so that clear cross-strand NH–H2 NOEs can be observed. The U_{33} NH proton resonance is weak and does not give rise to observable NOEs but its chemical shift at 13.8 ppm is consistent with that of a Watson–Crick A·U base-pair. A *J*(N, N)–HNN COSY experiment designed to yield cross-strand H2–N3 correlations from A·U base-pairs confirmed the presence of the U_{33}·A_{37} base-pair (Figure 6). Nucleotides A_{31}, A_{37}, and A_{38} also produce cross-strand H2–H1′ NOEs commonly observed for A·U base-pairs within helices.

The torsion angles of the sugar-phosphate backbone are within the limits of A-form geometry. The small (<5 Hz) H1′–H2′ couplings and the ^{13}C chemical shifts of the 3′ and 4′ resonances of nucleotides G_{28}–U_{32} and A_{38}–C_{43} are indicative of the C3′-*endo* sugar pucker typical of RNA helices. Small H4′-H5′/H5″ couplings for the nucleotides G_{29}–A_{31} and C_{40}–C_{42} indicate that their γ angles have the A-form *gauche*$^+$ conformation. The NOE intensities for residues with resolved H4′–H5′ and H4′–H5″ NOE cross-peaks also are consistent with the *gauche*$^+$ conformation. The majority of γ torsion angles from G_{27}–U_{32} and A_{38}–C_{43} are likely to be *gauche*$^+$, but due to spectral overlap, less than half of the angles of the stem could be confirmed. P–C2′ couplings indicate that the ε angles of G_{27}–U_{32} and A_{37}–C_{42} have the A-form *trans* conformation. The α angles (residues G_{28}–U_{32} and U_{39}–C_{43}) and the ζ angles (residues G_{27}–A_{31} and A_{38}–C_{42}) were loosely constrained to exclude the *trans* conformation, since all ^{31}P resonances of the stem cluster between −3.2 ppm and −4.5 ppm. None of the α or ζ angles within the converged structures deviated from *gauche*$^-$.

The U_{33} NH proton resonance has a chemical shift indicative of an A·U base-pair but is weakened by exchange with solvent and does not give rise to NOE cross-peaks. To address the possibility that the U_{33}·A_{37} base-pair constraint may lead to an alternative conformation of the lower stem or the loop, a third set of calculations was performed that imposed constraints for this base-pair. The structures resulting from this calculation are similar to those produced by calculations in which the A_{37}·U_{33} base-pair is not constrained except that the van der Waal's energies for the fragment from U_{33} to A_{37} increases ≈15 kcal/mol. In most of the structures, the U_{33}·A_{37} base-pair has a propeller twist of ≈32°. The magnitude of twist is not unexpected, since the U_{33}·A_{37} base-pair is the junction between the hairpin loop and the stem and planarity constraints were not imposed. Overall, the number of converged structures is greater without application of the U_{33}·A_{37} base-pair constraint and the loop is less compact, but the general features of the convergent are the same whether or not the base-pair is imposed.

Structure of $i^6A_{37}ACSL^{Phe}$

The dimethylallyl modification of $ACSL^{Phe}$ has only modest effects on the conformation of the RNA hairpin stem. NOE cross-peak intensities, ribose puckers, and sugar-phosphate backbone torsion angles in the stem region distal to the loop (G_{27}–A_{31} and U_{39}–C_{43}) are not affected by the modification of A_{37} and yield a structure analogous to that shown in Figure 9. The A_{38} H2 retains NOE cross-peaks to U_{33} H1′ and U_{39} H1′, but the NH resonance of U_{32} is weak. This suggests that the A_{37} modification partly disrupts the U_{32}·A_{38} base-pair and increases the solvent accessibility of the U_{32} NH proton. NOE cross-peaks from U_{33} H1′ to the H8 resonances of G_{34} and A_{35} also are retained in spectra of the modified RNA and are

Table 2. C6/8 and C1′ $T_{1\rho}$ relaxation times for ACSL^{Phe} and i^6A_{37} ACSL^{Phe} RNA molecules

	ACSL^{Phe} $T_{1\rho}$ (ms)				i^6A_{37} ACSL^{Phe} $T_{1\rho}$ (ms)		
Residue[a]	C1′	C6/C8	C2	Residue	C1′	C6/C8	C2
G_{27}	64.0	58.7		G_{27}	66.0	54.2	
G_{28}	60.9	55.7		G_{28}	62.4	53.9	
G_{29}	65.5	55.2		G_{29}	64.8	54.5	
G_{30}	64.5	55.5		G_{30}	68.4	53.5	
A_{31}	67.1	55.0	54.8	A_{31}	67.7	53.2	49.9
U_{32}	61.8	46.7		U_{32}	57.5	44.1	
U_{33}	61.6	44.4		U_{33}	n.m.[b]	51.4	
G_{34}	40.0	63.2		G_{34}	n.m.	64.7	
A_{35}	54.0	66.8	55.9	A_{35}	n.m.	66.2	59.6
A_{36}	41.0	51.2	55.7	A_{36}	n.m.	51.4	54.6
A_{37}	39.7	60.6	54.8	A_{37}	n.m.	51.2	
A_{38}	62.4	54.6	55.3	A_{38}	n.m.	50.5	52.4
U_{39}	67.1	47.1		U_{39}	64.9	43.5	
C_{40}	65.2	45.6		C_{40}	65.7	44.2	
C_{41}	67.1	44.3		C_{41}	67.7	42.7	
C_{42}	68.7	46.0		C_{42}	70.2	46.6	
C_{43}	75.0	49.5		C_{43}	78.8	47.9	

The uncertainty in the measured relaxation times is ±5%.
[a] The transcription reactions were primed with 5′-GMP, resulting in incomplete labeling of the 5′-terminal nucleotide and preventing the G_{27} C8 and C1′ relaxation rates from being measured.
[b] Not measured.

consistent with the lack of a U-turn (Figure 5(b)). Interestingly, the A_{37} H8 chemical shift changes only ≈0.1 ppm relative to the unmodified form of ACSL^{Phe}.

The A_{36} H8 and A_{37} H1′ are broad, leading to weak base–ribose NOE connectivities. The A_{36} H2 has a weak cross-peak to A_{37} H1′ consistent with stacking of the A_{36} base beneath A_{37} as in the unmodified molecule. The only distinguishable inter base NOE cross-peaks for residues 32–38 are U_{32} H6 to U_{33} H6 and U_{32} H5 to U_{33} H5 which are present only below 12 °C. The relative lack of inter-base cross-peaks suggests that the loop nucleotide bases do not stack on one another above 12 °C in a stable fashion as they do in the unmodified RNA molecule. The line widths for these base proton resonances range from 14 to 28 Hz and should not prevent observation of the NOE. Indeed, the U_{33} H5 and H6 and the A_{37} H1′ resonances are ≈28 Hz wide but still give rise to NOE cross-peaks. Thus, although the conformational changes resulting from dimethylallyl modification of A_{37} are modest, the dynamic changes of the RNA hairpin are pronounced.

The dimethylallyl functional group lies across the minor groove of the stem and is approximately coplanar with the bases of U_{33} and A_{37} (Figure 10(b)). The conformation of the dimethylallyl group is restricted by NOEs to U_{32}, U_{33}, G_{34}, and A_{38}. Strong cross-peaks from the CH_3 resonances to U_{33} H4′ and U_{32} H2′ are present in 2D NOESY and 3D ^{13}C-edited NOESY spectra. The CH_2 proton resonances have weak NOE cross-peaks to the resonances H5 and H6 of U_{32} and U_{33} and H2 of A_{38}. All protons of the dimethylallyl have NOE cross-peaks to the A_{37} secondary amine resonance at 320 ms mixing time.

Dynamics of the ACSL^{Phe} hairpins

The reorientation of a $^{13}C-^1H$ bond vector on the picosecond time-scale can be assessed through its carbon $T_{1\rho}$ relaxation: the longer the relaxation time, the more mobile the $^{13}C-^1H$ pair. The $T_{1\rho}$ relaxation times for the adenine C2, base C6/8, and ribose C1′ positions for ACSL^{Phe} and i^6A_{37} ACSL^{phe} are listed in Table 2. In ACSL^{Phe}, the C1′ relaxation times of residues G_{34} to A_{37} are significantly shorter than those of the stem residues (Table 2). Although weak, these resonances are clearly observed in the 66 ms constant-time HSQC spectrum and their linewidths indicate that they are not in intermediate exchange. Thus, relative to residues in the stem, the ribose sugars of the loop nucleotides appear more rigid. In i^6A_{37} ACSL^{phe}, the loop nucleotide sugar resonances are in intermediate exchange and their $T_{1\rho}$ relaxation times could not be accurately measured. However, the relaxation times for the stem nucleotide C1′ resonances of the modified RNA are similar to those of the unmodified molecule (Table 2). G_{34} and A_{35} have the longest C8 relaxation times of all C8 nuclei in both the unmodified and modified molecules. This is consistent with the loop-terminal locations of G_{34} and A_{35} in the structures calculated for ACSL^{Phe}. Since base stacking occurs on neither face of A_{35} and only one face of G_{34}, these residues would be expected to be the most flexible. The $T_{1\rho}$ relaxation time of A_{36} C8 also is similar in both molecules and suggests that stacking restricts the mobility of the A_{36} base. In the modified molecule, the U_{33} H6–C6 resonance pair undergoes chemical exchange and results in two sets of broad resonances for the U_{33} base. With the exception of A_{37}, which is extremely broad and its apparent relaxation dominated by chemical exchange, the

adenine C2 $T_{1\rho}$ relaxation times are essentially identical for $ACSL^{Phe}$ and i^6A_{37} $ACSL^{Phe}$ (Table 2). These relaxation times are slightly longer than relaxation times of adenine bases participating in Watson–Crick base-pairs reported for comparably sized RNA molecules.[32]

Effects of Mg^{2+} on the RNA hairpins

Mg^{2+} plays a fundamental role in organizing structural motifs of RNA molecules and stabilizing their conformations, including those of tRNA molecules.[6,33] The $ACSL^{Phe}$ and i^6A_{37} $ACSL^{Phe}$ molecules were tested for their ability to bind Mg^{2+} and to explore possible Mg^{2+}-induced conformational effects. Mg^{2+} weakens the intensity of the U_{32} and U_{33} NH resonances of $ACSL^{Phe}$ and leads to a downfield shift of the U_{32} NH proton resonance (Figure 3(c)). The NH resonances of G_{28}, G_{29}, and G_{30} exhibit small changes in chemical shift and intensity and the G_{34} resonance is extremely broadened. The U_{39} NH resonance is broadened and shifted upfield 0.3 ppm. The chemical shift effects at G_{27}–G_{30} are consistent with binding of divalent metal ions to triplets of G·C base-pairs.[34] The non-exchangeable resonances also exhibit spectral changes. The base 6 and 8 resonances of nucleotides U_{32} to A_{38} are broadened. The three uridine H5 and the adenine H2 nuclei give rise to two sets of resonances with an intensity ratio of ≈1:1 at a Mg^{2+} concentration <1 mM, but the increases to 2:1 between 5 and 20 mM. The chemical shifts of the weaker set of resonance correspond to the Mg^{2+}-free form of the hairpin.

For i^6A_{37} $ACSL^{Phe}$, addition of Mg^{2+} leads to extreme broadening of the U_{39} NH resonance, leaving only the G_{28}, G_{29}, and G_{30} NH resonances. The H5 resonances of the three uridines and the H6 resonance of U_{33} sharpen in the presence of Mg^{2+} and none of the resonances are doubled. The U_{33} H5 resonance is the most dramatically changed with its half-height linewidth decreasing from ≈90 Hz to 30 Hz. The methyl proton resonances of the dimethylallyl group sharpen when Mg^{2+} is present and lead to more intense U_{33} H1′-methyl and A_{38} H2-methyl NOE cross-peaks. The presence of Mg^{2+} also leads to correlations between A_{38} H2 and the CH and CH_2 resonances of the dimethylallyl group. Since the line widths of the resonances involved are substantially sharpened by Mg^{2+}, it is not clear whether these intensity changes reflect conformational differences between Mg^{2+}-free and Mg^{2+}-bound forms.

Although Mg^{2+} causes different resonance broadening patterns for $ACSL^{Phe}$ and i^6A_{37} $ACSL^{Phe}$, the spectra also share some features. Mg^{2+} does not significantly alter the intensities of the sequential NOE correlations with the exception of the U_{33} H1′–A_{35} H8 and U_{33} H2′–A_{35} H8 cross-peaks which become more intense. Mg^{2+} induces small chemical shift changes for peaks corresponding to stem residues G_{27}–G_{30} and C_{41}–C_{43}. The C_{40} H6 and A_{38} H2 resonances shift downfield 0.12 ppm and 0.20 ppm, respectively, and the U_{39} H1′ shifts upfield 0.17 ppm. The conformation of the sugar-phosphate backbone also does not appear to change appreciably in the presence of Mg^{2+}. Comparison of ^{31}P spectra of both molecules collected at 5 °C reveals that only a single broad resonance appears in the downfield region upon addition of 7 mM Mg^{2+}. This resonance, which could not be assigned for either molecule, is not observed at elevated temperatures. The presence of such a resonance is consistent with the adoption of the *trans* conformation of an α or ζ torsion angle,[29] but could also result from electrostatic factors such as the proximity of the phosphate to Mg^{2+}.

Discussion

Base modification of transfer RNA molecules occurs in all cells but the conformational and thermodynamic effects of many of these modifications within the stems and loops of tRNAs remain largely uncharacterized. Base modification at position 37 in the anticodon stem-loop of tRNAs is believed to stabilize tRNA·mRNA interactions by improving intrastrand stacking within tRNA anticodon loops and interstrand stacking between codon and anticodon bases. The anticodon stem-loop of *E. coli* $tRNA^{Phe}$ serves as a model to probe the physical effects of dimethylallyl modification.

The unmodified anticodon stem-loop lacks a U-turn

The unmodified anticodon stem-loop of *E. coli* $tRNA^{Phe}$ is surprisingly well structured. The stem is an A-form helix that includes base-pairs U_{32}·A_{38} and U_{33}·A_{37}. The non-exchangeable resonances of U_{33} and A_{37} do not exhibit characteristics of intermediate exchange as does the U_{33} NH resonance. This localization suggests that the NH proton undergoes slow to intermediate exchange with water protons and is partially exposed to solvent. Thus, the U_{33}·A_{37} base-pair is solvent accessible, but appears to be stable in its helix-terminal position.

The loop of the RNA hairpin contains only three nucleotides—G_{34}, A_{35}, and A_{36}. The 5′ base stack of the helix continues into the loop, with the G_{34} base stacking on the U_{33}·A_{37} base-pair and having a normal A-form geometry (Figure 10(a)). The A_{35} base stacks partially beneath A_{36} and the U_{33}·A_{37} base-pair and is co-planar with G_{34}. The A_{35} base points out of the helix and is tilted ≈25° relative to the base of G_{34}. The base of A_{36} is shifted into the minor groove pointing towards the helix axis, and does not stack directly beneath A_{37}. The loop appears to be stabilized primarily by stacking and hydrophobic interactions, since there is no spectral evidence of hydrogen bonding among the anticodon bases. The C2′-*endo* sugar puckers of each

of the three anticodon nucleotides also may permit formation of the stable loop. The long $T_{1\rho}$ relaxation times of the G_{34} and A_{35} C8 atoms (Table 2) indicate that these bases are more mobile (on the picosecond time-scale) than those of the stem and may occupy a greater region of space than suggested by the structure calculations (Figure 8). However, the $T_{1\rho}$ relaxation times do not provide direct information on the amplitudes of the nucleotide motions which may be small.

The conformation of the loop of the unmodified *E. coli* $ACSL^{Phe}$ is not the canonical U-turn motif. The $ACSL^{Phe}$ yields an NOE pattern similar to patterns observed for other anticodon loop sequences reported to contain U-turns, such as fully modified yeast $tRNA^{Phe}$, $tRNA^{Met}$, and $tRNA^{Lys}$.[35–37] In a U-turn, the sequential U_{33} H1′ to G_{34} H8 distance is ≥ 6 Å and would lead to a break of 1′-base NOE connectivities, whereas the non-sequential U_{33} H1′ to A_{35} H8 distance is 3.7 Å and should give rise to a moderately intense NOE. For the $ACSL^{Phe}$, the sequential 1′-base NOEs are continuous, albeit weak at the U_{33}–G_{34} step, and the non-sequential U_{33}–A_{35} interaction is present, but very weak. The NOEs predicted for a molecule containing a U-turn are a subset of the NOEs observed for the unmodified $ACSL^{Phe}$ and do not conflict with the stacked conformation of G_{34} and U_{33}. However, key NOEs present in the spectra of the $ACSL^{Phe}$ (U_{33} H1′–A_{38} H2, G_{34} H1′–A_{37} H2, and A_{35} H5′–A_{36} H2) are not compatible with the U-turn motif. These NOEs lead to a loop structure in which the phosphate backbone does not turn abruptly between U_{33} and G_{34}, as observed in the crystalline form of yeast $tRNA^{Phe}$, but instead turns between G_{34} and A_{35}. The turn of the phosphate backbone is maintained even when the unusual α and ζ torsion angles observed for the U-turn motif are applied during the constrained MD simulations.

i^6A_{37} modification alters the stability of the anticodon loop

Prenylation of A_{37} N6 increases the solvent accessibility of the NH protons proximal to the anticodon loop as evidenced by weakening of the U_{32}, U_{33}, and U_{39} NH resonances. Broadening of base and sugar-phosphate backbone resonances of nucleotides in and near the loop indicate that prenylation destabilizes the structure of this region of the ACSL and increases nucleotide mobility. Although the loop and loop-proximal nucleotide resonances are broadened, the relative NOE intensities in this region of the hairpin are largely unchanged. For example, NOE cross-peaks U_{33} H1′–G_{34} H8 and U_{33} H1′–A_{38} H2 indicate that the A-form geometry of the stem is conserved up to the anticodon in both molecules. The intra-residue NOE cross-peaks A_{37} H8–H2′ and A_{35} H8–H2′ are intense in both molecules as is the inter-residue A_{36} H2–A_{35} H4′ cross-peak. The increased mobility in this region appears to be the result of steric clash between the modification and cross-strand nucleotides. The position of the dimethylallyl group in the helix leads to NOEs from dimethylallyl methyl protons to U_{32} and U_{33} base protons and disrupts the U_{33}·A_{37} base-pair (Figure 10(b)). Thus, while the i^6A_{37} modification increases the dynamics of nucleotides within the loop region, the basic fold of the modified RNA hairpin remains largely unchanged.

Mg^{2+} can alter RNA conformation and stabilize tRNA tertiary structure.[6,33] Despite these properties, Mg^{2+} destabilizes the conformation of this hairpin loop. The Mg^{2+} dependent exchange broadening of loop and loop-proximal resonances in $ACSL^{Phe}$ is consistent with one or more low affinity binding sites. Interestingly, Mg^{2+} binding and dimethylallyl modification appear to cause similar changes in the loop region of the $ACSL^{Phe}$. The spectra of i^6A_{37} $ACSL^{Phe}$ and Mg^{2+}-bound $ACSL^{Phe}$ share many features, including resonance broadening patterns, resonance specific chemical shift changes, and relative NOE cross-peak intensities. However, the effects of Mg^{2+} and prenylation are not additive. Mg^{2+} sharpens resonances of the modified RNA hairpin and eliminates resonance doubling. This suggests that the combined effects of dimethylallyl modification and Mg^{2+} binding may be synergistic, promoting the formation of a structure that is not achieved by either effector individually. The reduced U_{33} H1′–G_{34} H8 NOE intensity combined with the enhanced U_{33} H1′–A_{35} H8 NOE intensity does suggest the loop conformation begins to favor a canonical U-turn motif, but remains dynamic.

Implications for modification of $ACSL^{Phe}$ by MiaA

Comparison of the primary structures of tRNA molecules containing the i^6A_{37} modification reveals conserved nucleotides at several positions in the stem and loop.[10,23] Nucleotides A_{36}, A_{37}, and A_{38} and the G_{30}·C_{40} base-pair are common to all the tRNA substrates of MiaA. Also, base-pair G_{29}·C_{41} is present in eight of nine tRNAs and the 31·39 base-pair is either A·ψ or U·A. The importance of base conservation at these sites has been probed by analyzing of the modification properties of MiaA from crude cell extracts and recombinant MiaA protein.[10,23] These studies demonstrate that the A_{36}–A_{37}–A_{38} motif is essential for MiaA modification and that base-pairs G_{29}·C_{41} and G_{30}·C_{40} enhance modification by MiaA. The nucleotide identity of the 31·39 base-pair does not significantly impact efficiency of MiaA when only the stem-loop is used as a substrate.[23] However, changing A_{31}·U_{39} of full-length unmodified $tRNA^{Phe}$ to other base-pairs decreases the k_{cat}/K_m for MiaA prenylation by 23- to 55-fold compared to that of the wild-type (M. Winkler, in preparation).

The structure of $ACSL^{Phe}$ indicates that MiaA may alter the conformation of nucleotides in the loop region prior to modification. Substitution

with guanine at positions 36 or 38 demonstrate the central role of A_{36} and A_{38} in MiaA recognition. The solution structure of $ACSL^{Phe}$ suggests that only a small degree of structural perturbation would be caused by G_{36} or G_{38} substitution, thus highlighting the importance of base functional groups for MiaA recognition. A_{36} should be freely accessible to MiaA, but A_{37} and A_{38} are in Watson–Crick base-pairs and the N1 and N6 functional groups are sequestered. Although the dimethylallyl group on i^6A_{37} points into the major groove and appears to leave the bridging hydrogen of the A_{37}·U_{33} base-pair in place (Figure 10(b)), the limited accessibility of this region in the native state would impede reaction of N6 with DMAPP unless the conformation of the loop is relaxed by MiaA.

The conservation of the 31·39 base-pair (A·ψ or U·A) does not appear to impart unique structural features to the loop or loop-proximal stem. In the unmodified $ACSL^{Phe}$, the A_{31}·U_{39} base-pair stacks between adjacent base-pairs and the continuity of the stem A-form geometry is maintained. A G_{31}·C_{39} base-pair should be able to substitute structurally for the A·U. Thus, the conservation of this base-pair may reflect a thermodynamic limitation on the loop. Since A_{38} is necessary for MiaA modification (and presumably recognition) a G_{31}·C_{39} base-pair may impede disassembly of the loop and access to the A_{36}–A_{37}–A_{38} motif.

Comparison to structures of other anticodon stem-loop sequences

Direct structural methods demonstrate that tRNA anticodon loops can fold into well-defined conformations or can be dynamic and presumably multi-conformational. The crystal structure of fully modified yeast $tRNA^{Phe}$ serves as the paradigm for the fold of the anticodon arm.[20,21] This fold consists of a five base-pair stem capped by a seven nucleotide loop. A U-turn created by a nearly 180° reverse of the phosphate backbone immediately 3′ to residue U_{33} and stacking of the anticodon nucleotide bases, residues 34, 35, and 36, on the 3′-side of the loop, characterize the loop conformation. The U-turn is stabilized by the anticodon base stack and by hydrogen bonds from U_{33} 2′OH to A_{35} N7 and from U_{33} N3H to the phosphoryl oxygen 3′ to A_{35}. The structural features of the yeast $tRNA^{Phe}$ anticodon arm are repeated in the conformations of native yeast $tRNA^{Asp}$[38] and native *E. coli* $tRNA^{Cys}$ complexed with EF-Tu and GDPNP.[39] Unlike yeast $tRNA^{Phe}$, however, the anticodon bases of these tRNAs are complementary and pair with one another to form an intermolecular helix within the crystal lattice. Pairing of anticodon loop bases to form intermolecular minihelices is a theme repeated for other native tRNA–protein complexes even when the anticodon bases do not have Watson–Crick complementarity.[40] These intermolecular base-pairs undoubtedly contribute stability to the anticodon loop conformations, but the degree to which the base modifications facilitate or stabilize these interactions is unclear.

Solution studies show that the general motif of the anticodon arm adopted by the crystalline form yeast $tRNA^{Phe}$ is one of several structures that tRNA anticodon arms can adopt. In solution, the loops of modified yeast $tRNA^{Phe}$ and human $tRNA^{Lys,3}$ and of unmodified *E. coli* initiator and elongator $tRNA^{Met}$ are composed of seven nucleotides.[35–37] The conformations adopted by these anticodon arms are similar to that of crystalline yeast $tRNA^{Phe}$ and are independent of Mg^{2+}. The anticodon arms of unmodified and ψ_{39} modified $tRNA^{Lys,3}$ also have five base-pair stems and seven nucleotide loops but lack well-defined U-turn motifs. Interestingly, the anticodon stems of yeast $tRNA^{Phe}$, human $tRNA^{Lys,3}$, and *E. coli* $tRNA^{Met}$ cannot form Watson–Crick base-pairs between residues 32 and 38. Protonation of A_{38} and formation of an C_{32}·A^{+}_{38} base-pair at pH 5.6 in human $tRNA^{Lys,3}$ increases the stem to six base-pairs and results in a three or five nucleotide loop.[37,41] The introduction of the N6-threonylcarbamoyl A_{37} modification into human $tRNA^{Lys,3}$ reinforces the five nucleotide loop and enhances base stacking on the 3′-side of the loop.[41]

Significance of the dimethylallyl modification for translation

In *E. coli* $tRNA^{Phe}$, thiolation followed by methylation at C2 of A_{37} requires the dimethylallyl modification at N6. Genetic studies using *E. coli* strains that are unable to carry out the N6 modification demonstrate the importance of the $ms^2i^6A_{37}$ tRNA modifications. Defects including decreased polypeptide chain elongation rates[12–14] and decreased efficiency of translation[14,22] characterize *E. coli* strains lacking these modifications.

In vitro[42] and *in vivo*[43,44] experiments designed to probe codon selection within the ribosome implicate the dimethylallyl group as the primary contributor to suppressor efficiency, to codon context sensitivity, and to the rate of protein synthesis. Hydrophobic modifications, such as the dimethylallyl group, often are present at residue 37 when residues 35 and 36 are A or U and are believed to increase stacking within the codon–anticodon minihelix.[10,45] On the basis of kinetic and thermodynamic properties of anticodon–anticodon minihelix formation between *E. coli* $tRNA^{Cys}$ (containing $ms^2i^6A_{37}$) and *E. coli* $tRNA^{Ala}$ and between yeast $tRNA^{Cys}$ (containing i^6A_{37}) and *E. coli* $tRNA^{Ala}$, Houssier & Grosjean concluded that the 2-thiomethyl functionality of $ms^2i^6A_{37}$ is the primary contributor to helix stability.[46,47] However, the degree of stabilization that the dimethylallyl group affords helices formed by *E. coli* $tRNA^{Phe}$ has not been directly established. *E. coli* $tRNA^{Cys}$ contains cytidine at position 35 rather than adenine and may further favor a closed loop conformation. Our results demonstrate that in

the absence of the 2-thiomethyl modification the dimethylallyl group relaxes the compact loop but does not result in stacking of the G_{34}–A_{37} bases and exposition of the base-pair functional groups. It is possible that the 2-thiomethyl modifications alone or in combination with the dimethylallyl modification further relaxes or opens the loop and exposes the Watson–Crick faces of the anticodon nucleotides, thereby reducing the thermodynamic barrier to helix formation. Thus the thiomethyl group may produce a stable minihelix by improving base stacking of the codon–anticodon base-pairs or by altering the conformation of the anticodon loop prior to helix formation. The latter mechanism offers the possibility that the dimethylallyl group may also function to stabilize stacking interactions of the codon–anticodon minihelix.

The destabilization effect of the dimethylallyl modification may have functional relevance for codon selection that extends beyond predisposing the anticodon bases to rearrangement upon ribosome binding and involves disruption of the U_{32}·A_{38} base-pair. *Mycoplasma mycoides* $tRNA^{Gly}_{UCC}$ is unusual in that it exhibits an extended wobble effect by efficiently recognizing all four glycine codons rather than only GGG and GGA codons. *E. coli* $tRNA^{Gly}_{1}$ and a variant, $tRNA^{Gly}_{1\text{-}UCC}$ that has the anticodon (CCC) replaced with (UCC), obey the standard wobble rules.[48] These *E. coli* tRNAs are not modified at positions 32, 33, 37 and 38 but have the same nucleotide bases at these positions as *E. coli* $tRNA^{Phe}$. Substitution of U_{32} with C to create a C_{32}–A_{38} mismatch in the stem of $tRNA^{Gly}_{1\text{-}UCC}$ causes an extended wobble effect, analogous to *M. mycoides* $tRNA^{Gly}_{UCC}$.[49] This substitution also increases −1 frameshifting at GGA codons.[48–50] If U_{32} and A_{38} of $tRNA^{Gly}_{1\text{-}UCC}$ form a Watson–Crick base-pair analogous to that of unmodified $tRNA^{Phe}$, then substitution with C at position 32 would break the 32·38 interaction. For *E. coli* $tRNA^{Phe}$ *in vivo*, lack of the N6 and C2 modifications, and presumably retention of the ψ_{32}·A_{38} base-pair, reduces the wobble effect[43] and increases +1 frameshifting.[51] Thus, the presence of the 32·38 base-pair appears to limit wobbling and influence frameshifting in $tRNA^{Gly}_{1\text{-}UCC}$ and in *E. coli* $tRNA^{Phe}$ with unmodified A_{37}. Although the contribution to translational fidelity or 32·38 base-pair stability of the A_{37} 2-thiomethyl modification in *E. coli* $tRNA^{Phe}$ has not been examined, the $U_{32} \rightarrow \psi$ modification has minimal impact.[52] Thus, the prenyl group at A_{37} may enable wobbling and reduce +1 frameshifting by relaxing the closed loop that sequesters the anticodon bases and enhance codon–anticodon recognition.

Materials and Methods

All enzymes were purchased from Sigma Chemical, except for T7 RNA polymerase and MiaA enzymes, which were prepared as described.[53,54] Deoxyribonuclease I type II, pyruvate kinase, adenylate kinase, and nucleotide monophosphate kinase were obtained as powders, dissolved in 15% (v/v) glycerol, 1 mM dithiothreitol, and 10 mM Tris–HCl (pH 7.4), and stored at −20 °C. Guanylate kinase and nuclease P1 were obtained as solutions and stored at −20 °C. Unlabeled 5′ nucleoside triphosphates (5′-NTPs) were purchased from Sigma, phosphoenolpyruvate (potassium salt) was purchased from Bachem, and 99% [^{15}N]ammonium sulfate and 99% [^{13}C]methanol were purchased from Cambridge Isotope Labs. γ,γ-Dimethylallyl diphosphate was purchased from Sigma.

Preparation of RNA samples

The RNA sequence for *E. coli* $ACSL^{Phe}$ shown in Figure 1 was synthesized *in vitro* using T7 RNA polymerase and a synthetic DNA template. The nucleotide sequence of the stem corresponds to residues G_{27} to C_{43} of full-length *E. coli* $tRNA^{Phe}$. Unlabeled RNA molecules were prepared from 10 ml transcription reactions using 4 mM 5′-NTPs. Isotopically labeled RNA molecules were prepared from 10 ml transcription reactions using 3 mM uniformly ^{15}N-enriched and ^{13}C-enriched 5′-NTPs as described.[55,56] The RNA molecules were purified by passage through 20% (w/v) preparative polyacrylamide gels, electroeluted (Schleicher & Schuell), and precipitated with ethanol. The purified oligonucleotides were dissolved in 1.0 M NaCl, 20 mM potassium phosphate (pH 6.8) and 2.0 mM EDTA, and dialyzed extensively against 10 mM NaCl, 10 mM potassium phosphate (pH 6.8) and 0.05 mM EDTA, using a Centricon-3 concentrator (Amicon Inc.). The samples were diluted with buffer to a volume of 200 μl and lyophilized to a powder. For experiments involving the non-exchangeable protons, the samples were exchanged twice with 99.9% ^2H_2O and then resuspended in 200 μl of 99.96% ^2H_2O. For experiments involving detection of the exchangeable protons, the samples were resuspended in 200 μl of 90% H_2O/10% ^2H_2O. The samples contained 50–130 A_{260} OD units of unmodified RNA oligonucleotide in 200 μl (Å1.7–4.3 mM) and 75–100 A_{260} OD units of modified RNA oligonucleotide (≈2.5–3.4 mM). For experiments involving detection of ^{31}P, the 5′-terminal phosphate was removed by treatment with alkaline phosphatase (0.47 U/pmol of $ACSL^{Phe}$) as described.[57]

Preparation of the A_{37} (N6)-dimethylallyl modified $ACSL^{Phe}$

The dimethylallyl modification was introduced at position A_{37} of purified $ACSL^{Phe}$ using the enzyme MiaA dimethylallyl diphosphate:tRNA transferase (MiaA) and DMAPP. Histidine-tagged MiaA was expressed in *E. coli* and purified using Ni^{2+} affinity resin as described.[53] The typical modification reaction was performed using 50 μM $ACSL^{Phe}$, 125 μM DMAPP, 50 mM Tris–HCl (pH 7.6), 10 mM $MgCl_2$, 0.1 mg/ml BSA, 5 mM β-mercapto ethanol, and 26 μg/ml MiaA. The reactions were incubated overnight at 30 °C. Upon completion, the solution was extracted with cold phenol:chloroform:isomayl alcohol (25:24:1) and chloroform, and the RNA precipitated with ethanol. The reactions were monitored using 20% denaturing PAGE and proceeded to ≥95% completion. The modified $ACSL^{Phe}$ migrates slower than unmodified $ACSL^{Phe}$ and leads to a band shift equivalent to one additional nucleotide.

NMR spectroscopy

All NMR spectra were acquired on a Bruker AMX-500 spectrometer equipped with a ^{1}H-{X} broadband probe, except for the ^{31}P-decoupled ^{13}C–^{1}H constant time (ct) HSQC experiment, which was collected with a ^{1}H–{^{13}C, ^{31}P} triple resonance probe. Broadband decoupling of the carbon and nitrogen resonances was achieved using GARP with $\gamma B_2 = 3125$ Hz for carbon and $\gamma B_2 = 1570$ Hz for nitrogen. H_2O spectra were collected at 12 °C with solvent suppression using either spin lock pulses or binomial $1\overline{1}$ or $1\overline{3}3\overline{1}$ read pulses with maximum excitation at 12.5 ppm. ^2H_2O spectra were collected at 25 °C with presaturation or spin lock pulses to suppress the residual H^2HO peak. Quadrature detection was achieved using the States-TPPI method, and acquisition was delayed by a half-dwell in all indirectly detected dimensions. Typically, the data points were extended by 25% using linear prediction for the indirectly detected dimensions and the data were apodized using 1 Hz line broadening and 65° shifted sinebell functions. ^{1}H spectra were referenced to DSS (0.00 ppm). References for the ^{13}C and ^{15}N spectra were calculated using the spectrometer frequencies as reported. The ^{31}P spectra were referenced to an external standard of TMP which was set at 0.00 ppm. All spectra were processed and analyzed with Felix 98.0 (Molecular Simulations, Inc.).

Two-dimensional ^{13}C–^{1}H HMQC and HSQC spectra were collected to identify ^{13}C–^{1}H chemical shift correlations. Two-dimensional HCCH-COSY and 3D HCCH-TOCSY (24 ms DIPSI-3 spin lock) experiments optimized for polarization transfer through the ribose carbon atoms and a 2D ^{13}C–^{1}H HCCH-TOCSY (52 ms DIPSI-3 spin lock) optimized for polarization transfer through the adenine bases were collected in ^2H_2O to identify ribose spin systems and H8–H2 correlations, respectively.[25,58] To identify intra-residue base-sugar correlations, a 2D ^{15}N–^{1}H HSQC experiment was acquired in ^2H_2O and optimized for two- and three-bond correlations as reported,[27] except that the ^{15}N–^{1}H anti-phase magnetization was refocused after the t_1 evolution period to achieve cross-peaks that were in-phase in ω_1 and ω_2 and to permit application of broad band ^{15}N decoupling during the t_2 acquisition period. A J(N, N)–HNN COSY experiment was acquired in ^2H_2O to confirm the presence of A·U base-pairs.[28]

Distance constraints for the non-exchangeable resonances of unmodified $ACSL^{Phe}$ were derived at 25 °C from 2D ^{1}H–^{1}H NOESY spectra (120, 180, 360, 480, and 520 ms mixing times), ^{13}C-edited 3D NOESY-HMQC spectra (180 and 360 ms mixing times), and ^{13}C-edited 3D NOESY-ctHSQC spectra (80, 180, and 360 ms mixing times) optimized for the ribose resonances in ω_2 and ω_3. Similar experiments were acquired for the non-exchangeable resonances of i^6A_{37} $ACSL^{Phe}$ except that 2D NOESY spectra were also collected at 12 °C, 18 °C, and 32 °C. For the exchangeable resonances, 2D ^{15}N–^{1}H HSQC spectra were collected to identify ^{15}N–^{1}H chemical shift correlations. Two-dimensional ^{1}H–^{1}H NOESY experiments optimized for imino (NH) proton resonances in ω_2 were acquired at 60 and 360 ms mixing time in 90% H_2O to obtain distance restraints involving the exchangeable protons.

Backbone torsion angle constraints were derived from ^{1}H–^{1}H, ^{31}P–^{1}H, and ^{13}C–^{31}P coupling constants obtained from the following experiments. A ^{31}P-decoupled DQF-COSY experiment and a 2D HetCor experiment were acquired in ^2H_2O with unlabeled RNA samples. Three-bond ^{31}P–^{13}C coupling constants were measured using a pair of 2D ^{13}C–^{1}H ctHSQC experiments with and without ^{31}P decoupling in t_1.[59]

^{13}C $T_{1\rho}$ relaxation times were measured using 2D ^{13}C–^{1}H ctHSQC based experiments[60] separately optimized for C2, C6/8, and C1′ regions by centering the ^{13}C carrier at 152.6 ppm, 134.8 ppm, and 90.2 ppm, respectively. A 2.3 kHz ^{13}C spin lock field was used with delays of 4, 8, 12, 16, 24, 60, and 80 ms and 4, 8, 12, 16, 24, 44, 60, 80, and 120 ms for the C6/8 and C1′ measurements, respectively. The 12 and 24 ms experiment were collected twice to provide an estimate of the error of the measured intensities. The ^{13}C–^{1}H cross-peak volumes were fit to a single exponential decay.

Interproton distance constraints

Semi-quantitative distance constraints between non-exchangeable protons were estimated from cross-peak intensities in 2D NOESY and 3D ^{13}C-edited NOESY spectra. Using the covalently fixed pyrimidine H5–H6 distance (2.4 Å) and the conformationally restricted sugar H1′–H2′ distance (2.8–3.0 Å) as references, peak intensities were classified as strong, medium, weak, or very weak and their corresponding proton pairs given upper bound distance constraints of 3.0, 4.0, 5.0, or 6.0 Å, respectively. Cross-peaks observed only at mixing times $\geq$180 ms were classified as extremely weak and given 7.0 Å upper bound distance constraints to account for the possibility of spin diffusion. To improve convergence of the calculations, all distance constraints were given lower bounds of 0.0 Å. Distance constraints involving exchangeable protons were estimated from 360 ms mixing time NOESY spectra and were classified as either weak, very weak, or extremely weak, except for the intra-base-pair distances A·U H2–NH and G·C NH–NH_2, which were classified as strong constraints. Only intra-residue sugar-to-sugar constraints involving H5′ and H5″ resonances were included in the calculations.

An initial set of structures was calculated using a shortened version of the simulated annealing protocol (described below). A list of all proton pairs in the calculated structures closer than 5.0 Å (representing expected NOEs) was compared to the list of constraints. The NOESY spectra were then re-examined for predicted NOEs absent from the constraint list. In some cases, this allowed the unambiguous assignment of previously unidentified NOEs, but, in other cases, the predicted NOEs were unobservable due to spectral overlap or the broadening of resonances by exchange with solvent. After the final calculations, virtually all predicted NOEs not in the list could be accounted for by spectral overlap or exchange broadening. No NOEs could be observed, however, for proton pairs U_{33} H1′–A_{37} H2 and A_{35} H1′–A_{36} H5′ that were consistently found to be closer than 3.0 Å in calculated structures. One possible explanation for this is that the U_{33} and A_{35} ribose puckers were unconstrained and 2′-*endo* constrained, respectively. The A_{35} H1′–H2′ coupling constant suggests this riboses has some 3′-*endo* character (see Table 5 of Supplementary Material) which would increase the H1′–H5′ interproton distance and thus reduce the intensity of the potential NOE.

Hydrogen bonding constraints

Watson–Crick base-pairs were identified using two criteria: the observation of a significantly downfield

shifted NH or NH_2 proton resonance and the observation of strong G·C NH–NH_2 or A·U H2–NH NOEs. The A_{37}·U_{33} base-pair was identified by observation of a cross-peak between A_{37}H2 and U_{33}N3 in the J(N, N)–HNN COSY spectrum. Hydrogen bonds were introduced as distance restraints of 2.9 ± 0.3 Å between donor and acceptor heavy atoms and 2.0 ± 0.2 Å between acceptor and hydrogen atoms. Constraints identified in this way were included in the calculations for base-pairs G_{27}·C_{43}, G_{28}·C_{42}, G_{29}·C_{41}, G_{30}·C_{40}, A_{31}·U_{39}, and U_{32}·A_{38}. The U_{33}·A_{37} base-pair constraint was set to 2.9 ± 1.2 Å and 2.0 ± 1.2 Å between donor and acceptor heavy atoms and acceptor and hydrogen atoms, respectively, to permit conformational freedom of loop residues.

Dihedral angle constraints

Constraints on the ribose ring and backbone dihedral angles were derived from semi-quantitative measurements of $^3J_{H-H}$, $^3J_{H-P}$, and $^3J_{C-P}$ couplings.[32,61] Sugar pucker conformations were determined from $^3J_{H1'-H2'}$ couplings in ^{31}P-decoupled 2D DQF-COSY spectra. Residues with H1′–H2′ couplings >7 Hz were constrained to the C2′-*endo* conformation through two of the torsion angles in the ribose sugar ring.[31] Independent confirmation of sugar pucker conformation was provided by the observation of weak (<5 Hz) $^3J_{H3'-H4'}$ couplings, C3′ resonances shifted downfield to 76–80 ppm from the main cluster at 70–72 ppm, and C4′ resonances shifted downfield to 85–86 ppm from the main cluster at 82–84 ppm. Residues with weak (<5 Hz) $^3J_{H1'-H2'}$ couplings and large (>5 Hz) $^3J_{H3'-H4'}$ couplings were constrained to the C3′-*endo* conformation. Residues with intermediate $^3J_{H1'-H2'}$ couplings were left unconstrained to reflect the possibility of conformational averaging.

Dihedral angle constraints for the γ torsion angle were derived from $^3J_{H4'-H5'}$ and $^3J_{H4'-H5''}$ couplings in the DQF-COSY spectrum and intra-residue H4′–H5′ and H4′–H5″ cross-peak intensities in the 80 ms mixing time 3D NOESY-ctHSQC spectrum. For residues in which H4′–H5′ and H4′–H5″ peaks in the DQF-COSY spectra were clearly absent, representing couplings <5 Hz, γ was constrained to the gauche$^+$ conformation (60 ± 20°).[31,61] For residues with clear $^3J_{H4'-H5'}$ or $^3J_{H4'-H5''}$ couplings >5 Hz and unequal H4′–H5′ and H4′–H5″ NOE intensities, γ was constrained to include both the *trans* and *gauche*$^-$ conformations (−120 ± 120°), reflecting the lack of stereospecific assignments for the H5′ and H5″ resonances. For residues with only weak or unobservable $^3J_{H4'-H5'}$ or $^3J_{H4'-H5''}$ couplings and unequal H4′–H5′ and H4′–H5″ NOE intensities, γ was left unconstrained to reflect the possibility of conformational averaging.

Dihedral angle restraints for the β and ε torsion angles were derived from $^3J_{P-H5'}$, $^3J_{P-H5''}$, and $^3J_{P-H3'}$ couplings measured in 2D ^{31}P–^{1}H HetCor spectra and $^3J_{P-C2'}$ couplings measured in 2D ctHSQC spin-echo difference spectra. β was constrained to the *trans* conformation (180 ± 40°) for residues in which P–H5′ and P–H5″ peaks in the HetCor spectra were clearly absent, representing couplings <5 Hz.[31,61] For residues in which P–H5′ and P–H5″ peaks could be observed, β was left unconstrained to reflect the lack of stereospecific assignments and the possibility of conformational averaging. ε was constrained to the *trans* conformation (−150 ± 40°) for residues with $^3J_{P-H3'} > 5$ Hz and $^3J_{P-C2'} < 5$ Hz and to the gauche$^-$ conformation (−100 ± 40°) for residues with $^3J_{P-H3'} > 5$ Hz and $^3J_{P-C2'} > 5$ Hz.[31,61] Residues with $^3J_{P-H3'} > 5$ Hz but for which $^3J_{P-C2'}$ was not two standard deviations above 5 Hz were loosely constrained to include both conformations (−125 ± 65°).

Dihedral angle restraints for α and ζ were derived from the observation that a *trans* conformation of either dihedral angle is generally associated with a large downfield shift of the bridging ^{31}P resonance.[29] Because no such shift is observed for any of the ^{31}P resonances in the RNA molecules, α and ζ were loosely constrained to exclude the *trans* conformation (0 ± 120°) for all residues except those in the loop regions (nucleotides U_{33} to A_{37}), which were left unconstrained. No dihedral angle constraints were used for the glycosidic angle χ. A total of 46 restraints (10 α, 4 β, 5 γ, 15 ε, and 10 ζ) were used to constrain the phosphate backbone dihedral angles in the calculations.

Structure calculations

All calculations were carried out on Silicon Graphics O_2 work stations using X-PLOR 3.851.[62] The dihedral angles of a model structure (generated using Insight II, Molecular Simulations, Inc.) were randomized to generate 60 starting structures which were used in a simulated annealing/restrained molecular dynamics (rMD) routine.[31,32] The calculation protocol was divided into three stages: global fold, refinement, and final minimization. The global fold step consisted of 1000 cycles of unconstrained steepest-descent energy minimization, 10 ps of rMD at 1000 K using only hydrogen bond and NOE constraints, 9 ps of rMD at 1000 K during which repulsive van der Waals forces were introduced, 14 ps of rMD while cooling to 300 K, and 1000 cycles of conjugate gradient constrained minimization. The structures were then refined with 500 cycles of constrained minimization, 5 ps of rMD at 1200 K during which the α, β, γ, ε, ζ and sugar ring dihedral constraints were slowly introduced followed by 5 ps of rMD while cooling to 300 K, and 1000 cycles of constrained minimization. The final minimization step consisted of 1000 cycles of energy minimization using all constraints and repulsive van der Waals potentials. To determine the consistency of the NMR data with different possible base-pairing schemes in the loop, three additional sets of calculations were performed: one with U_{33}·A_{37} base-pair constraints, one without U_{33}·A_{37} base-pair constraints, and one that included loop phosphate backbone torsion angle constraints using values derived from the X-ray crystal structure of fully modified yeast tRNA^{Phe} and no U_{33}·A_{37} base-pair constraints. These calculations were performed beginning with the coordinates of converged structures from the global-fold rMD simulation. Structures were viewed using Insight II (Molecular Simulations, Inc.).

Thermal stability

UV melting studies were performed using 2.2 μM RNA hairpin dissolved in NMR buffer (10 mM NaCl, 10 mM potassium phosphate (pH 6.8) and 0.05 mM EDTA). A_{260} absorbance spectra from 8–95 °C were acquired (1.0 °C per minute) on a Pharmacia Ultrospec 2000 UV–visible spectrophotometer equipped with a peltier melting apparatus. The melting curves were acquired in triplicate but could not be fit to a two-state model.

Protein Data Bank accession numbers

Atomic coordinates for the refined structures have been deposited with the Protein Data Bank under accession codes 1kka and 1j4y.

Acknowledgments

We thank T. Olson for assistance with resonance assignments of $ACSL^{Phe}$, M. Michnicka for preparation of the T7 RNA polymerase, Dr H. -C. E. Leung for providing the plasmid construct for the MiaA enzyme, and Dr D. G. Gorenstein for providing access to the Magnetic Resonance Facility at UTMB in order to perform the $^1H-\{^{13}C, ^{31}P\}$ triple resonance experiments. We also thank Dr E. DeJong for helpful discussions. This work was supported by grants from the Robert A. Welch Foundation (C1277) and the National Science Foundation (MCB-0078501) to E.P.N.

References

1. Björk, G. R. (1995). Biosynthesis and function of modified nucleosides. In *tRNA: Structure, Biosynthesis, and Function* (Söll, D. & RajBhandary, U., eds), ASM Press, Washington, DC.
2. Garcia, G. A. & Goodenough-Lashua, D. M. (1998). Mechanisms of modifying enzymes. In *Modification and Editing of RNA: The Alteration of RNA Structure and Function* (Grosjean, H. & Benne, R., eds), ASM Press, Washington, DC.
3. Winkler, M. E. (1998). Genetics and regulation of tRNA and rRNA modification. In *Modification and Editing of RNA: The Alteration of RNA Structure and Function* (Grosjean, H. & Benne, R., eds), ASM Press, Washington, DC.
4. Davis, D. R. (1998). Biophysical and conformational properties of modified nucleosides in RNA. In *Modification and Editing of RNA* (Grosjean, H. & Benne, R., eds), pp. 85–102, ASM Press, Washington, DC.
5. Dao, V., Guenther, R. H. & Agris, P. F. (1992). The role of 5-methylcytidine in the anticodon arm of yeast $tRNA^{Phe}$: site-specific Mg^{2+} binding and coupled conformational transitions in DNA analogs. *Biochemistry*, **31**, 11012–11019.
6. Agris, P. F. (1996). The importance of being modified: roles of modified nucleosides and Mg^{2+} in RNA structure and function. *Prog. Nucl. Acid Res. Mol. Biol.* **53**, 79–129.
7. Björk, G. R. (1998). Modified nucleosides at positions 34 and 37 of tRNAs and their predicted coding capacities. In *Modification and Editing of RNA* (Grosjean, H. & Benne, R., eds), pp. 577–582, ASM Press, Washington, DC.
8. Tsang, T. H., Buck, M. & Ames, B. (1983). Sequence specificity of tRNA-modifying enzymes: an analysis of 258 tRNA sequences. *Biochim. Biophys. Acta*, **741**, 180–196.
9. Moore, J. A. & Poulter, C. D. (1997). *Escherichia coli* dimethylallyl diphosphate:tRNA dimethylallyltransferase: a binding mechanism for recombinant enzyme. *Biochemistry*, **36**, 604–614.
10. Motorin, Y., Bec, G., Tewari, R. & Grosjean, H. (1997). Transfer RNA recognition by the *Escherichia coli* Δ^2-isopentenyl-pyrophosphate:tRNA Δ^2-isopentenyl transferase: dependence on the anticodon arm structure. *RNA*, **3**, 721–733.
11. Sprinzl, M., Horn, C., Brown, M., Ioudovitch, A. & Steinberg, S. (1998). Compilation of tRNA sequences and sequences of tRNA genes. *Nucl. Acids Res.* **26**, 148–153.
12. Diaz, I., Pedersen, S. & Kurland, C. G. (1987). Effects of *miaA* on translation and growth rates. *Mol. Gen. Genet.* **208**, 373–376.
13. Ericson, J. U. & Björk, G. R. (1991). tRNA anticodons with the modified nucleoside 2-methylthio-N^6-(4-hydroxyisopentenyl)adenosine distinguish between bases 3′ of the codon. *J. Mol. Biol.* **218**, 509–516.
14. Hagervall, T. G., Ericson, J. U., Esberg, B., Ji-nong, L. & Björk, G. R. (1990). Role of tRNA modification in translational fidelity. *Biochim. Biophys. Acta*, **1050**, 263–266.
15. Björnsson, A. & Isaksson, L. A. (1993). UGA codon context which spans three codons. Reversal by $ms^2i^6A_{37}$ in tRNA, mutation in *rpsD*(S4) or streptomycin. *J. Mol. Biol.* **232**, 1017–1029.
16. Bouadloun, F., Srichaiyo, T., Isaksson, L. A. & Björk, G. R. (1986). Influence of modification next to the anticodon in tRNA on codon context sensitivity of translational suppression and accuracy. *J. Bacteriol.* **166**, 1022–1027.
17. Connolly, D. M. & Winkler, M. E. (1989). Genetic and physiological relationships among the miaA gene, 2-methylthio-N6-(Δ^2-isopentenyl)-adenosine tRNA modification, and spontaneous mutagenesis in *Escherichia coli* K-12. *J. Bacteriol.* **171**, 3233–3246.
18. Petrullo, L. A., Gallagher, P. J. & Elseviers, D. (1983). The role of 2-methylthio-N6-isopentenyladenosine in readthrough and suppression of nonsense codons in *Eshcerichia coli*. *Mol. Gen. Genet.* **190**, 289–294.
19. Harrington, K. M., Nazarenko, I. A., Dix, D. B., Thompson, R. C. & Uhlenbeck, O. C. (1993). *In vitro* analysis of translational rate and accuracy with an unmodified tRNA. *Biochemistry*, **31**, 7617–7622.
20. Kim, S.-H., Suddath, F. L., Quigley, G. J., McPherson, A., Sussman, J. L., Wang, A. H. J. *et al.* (1974). Three-dimensional tertiary structure of yeast phenylalanine transfer RNA. *Science*, **185**, 435–440.
21. Robertus, J. D., Ladner, J. E., Finch, J. R., Rhodes, D., Brown, R. S., Clark, B. F. C. & Klug, A. (1974). Structure of yeast phenylalanine tRNA at 3 Å resolution. *Nature*, **250**, 546–551.
22. Vacher, J., Grosjean, H., Houssier, C. & Buckingham, R. H. (1984). The effect of point mutations affecting *Escherichia coli* tryptophan tRNA on anticodon–anticodon interactions and on UGA suppression. *J. Mol. Biol.* **177**, 329–342.
23. Soderberg, T. & Poulter, C. D. (2000). *Escherichia coli* dimethylallyl diphosphate:tRNA dimethylallyltransferase: essential elements for recognition of tRNA substrates within the anticodon stem-loop. *Biochemistry*, **39**, 6546–6553.
24. Cabello-Villegas, J. & Nikonowicz, E. P. (2000). Discriminating duplex and hairpin oligonucleotides using chemical shifts: application to the anticodon stem-loop of *Escherichia coli* $tRNA^{Phe}$. *Nucl. Acids Res.* **28**, E74.
25. Nikonowicz, E. P. & Pardi, A. (1993). An efficient procedure for assignment of the proton, carbon, and nitrogen resonances in $^{13}C/^{15}N$ labeled nucleic acids. *J. Mol. Biol.* **232**, 1141–1156.
26. Pardi, A. (1995). Multidimensional heteronuclear NMR experiments for structure determination of

isotopically labeled RNA. *Methods Enzymol.* **261**, 350–380.
27. Sklenar, V., Peterson, R. D., Rejante, M. R. & Feigon, J. (1994). Correlation of nucleotide base and sugar protons in a ^{15}N-labeled HIV-1 RNA oligonucleotide by ^{1}H–^{15}N HSQC experiments. *J. Biomol. NMR*, **4**, 117–122.
28. Henning, M. & Williamson, J. R. (2000). Detection of N—H···N hydrogen bonding in RNA *via* scalar couplingsin the absence of observable imino proton resonances. *Nucl. Acids Res.* **28**, 1585–1593.
29. Gorenstein, D. G. (1984). *Phosphorus-31 NMR: Principles and Applications*, Academic Press, New York.
30. Davisson, V. J., Woodside, A. B., Neal, T. R., Stremler, K. E., Muehlbacher, M. & Poulter, C. D. (1986). Phosphorylation of isoprenoid alcohols. *J. Org. Chem.* **51**, 4768–4779.
31. Varani, G., Aboul-ela, F. & Allain, F. H.-T. (1996). NMR investigation of RNA structure. *Prog. Nucl. Magn. Reson. Spectrosc.* **29**, 51–127.
32. Smith, J. S. & Nikonowicz, E. P. (1998). NMR structure and dynamics of an RNA motif common to the spliceosome branch-point helix and the RNA-binding site for GA coat protein. *Biochemistry*, **37**, 13486–13498.
33. Laing, L. G., Gluick, T. C. & Draper, D. E. (1994). Stabilization of RNA structure by Mg ions: specific and non-specific effects. *J. Mol. Biol.* **237**, 577–587.
34. Allain, F. H. & Varani, G. (1995). Structure of the P1 helix from group I self-splicing introns. *J. Mol. Biol.* **250**, 333–353.
35. Clore, G. M., Gronenborn, A. M., Piper, E. A., McLaughlin, L. W., Graeser, E. & van Boom, J. H. (1984). The solution structure of a RNA pentadecamer comprising the anticodon loop and stem of yeast tRNA^{Phe}. A 500 MHz ^{1}H-n.m.r. study. *Biochem. J.* **221**, 737–751.
36. Schweisguth, D. C. & Moore, P. B. (1997). On the conformation of the anticodon loops of initiator and elongator methionine tRNAs. *J. Mol. Biol.* **267**, 505–519.
37. Durant, P. C. & Davis, D. R. (1999). Stabilization of the anticodon stem-loop of tRNA^{Lys,3} by an A^{+}-C base-pair and by pseudouridine. *J. Mol. Biol.* **285**, 115–131.
38. Moras, D., Dock, A. C., Dumas, P., Westhof, E. & Romby, P. (1986). Anticodon–anticodon interaction induces conformational changes in tRNA: yeast tRNAAsp, a model for tRNA–mRNA recognition. *Proc. Natl Acad. Sci. USA*, **83**, 932–936.
39. Nissen, P., Thirup, S., Kjeldgaard, M. & Nyborg, J. (1999). The crystal structure of Cys-tRNA^{Cys}-EF-Tu-GDPNP reveals general and specific features in the ternary complex in tRNA. *Structure*, **7**, 143–156.
40. Bénas, P., Bec, G., Keith, G., Marquet, R., Ehresmann, C., Ehresmann, B. & Dumas, P. (2000). The crystal structure of HIV reverse-transcription primer tRNA^{Lys,3} shows a canonical anticodon loop. *RNA*, **6**, 1347–1355.
41. Stuart, J. W., Gdaniec, Z., Guenther, R. H., Marzalek, M., Sochacka, E., Malkiewicz, A. & Agris, P. F. (2000). Functional anticodon architecture of human tRNA^{Lys,3} includes disruption of intraloop hydrogen bonding by the naturally occurring amino acid modification t6A. *Biochemistry*, **39**, 13396–13404.
42. Gefter, M. L. & Russell, R. L. (1969). Role modifications in tyrosine transfer RNA: a modified base affecting ribosome binding. *J. Mol. Biol.* **39**, 145–157.
43. Persson, B. C., Esberg, B., Ólafsson, Ó. & Björk, G. R. (1994). Synthesis and function of isopentenyl adenosine derivatives in tRNA. *Biochimie*, **76**, 1152–1160.
44. Esberg, B. & Björk, G. R. (1995). The methylthio group (ms2) of N6-(4-hydroxyisopentenyl)-2-methylthioadenosine (ms^{2}io^{6}A) present next to the anticodon contributes to the decoding efficiency of the tRNA. *J. Bacteriol.* **177**, 1967–1975.
45. Cedergren, R. J., Sankoff, D., LaRue, B. & Grosjean, H. (1981). The evolving tRNA molecule. *Crit. Rev. Biochem. Mol. Biol.* **11**, 35–104.
46. Houssier, C. & Grosjean, H. (1985). Temperature jump relaxation studies on the interactions between transfer RNAs with complementary anticodons. The effect of modified bases adjacent to the anticodon triplet. *J. Biomol. Struct. Dyn.* **3**, 387–408.
47. Grosjean, H., Houssier, C., Romby, P. & Marquet, R. (1998). Modulation role of modified nucleotides in RNA loop-loop interaction. In *Modification and Editing of RNA* (Grosjean, H. & Benne, R., eds), pp. 113–134, American Society for Microbiology Press, Washington, DC.
48. Lustig, F., Borén, T., Claesson, C., Simonsson, C., Barciszewska, M. & Lagerkvist, U. (1993). The nucleotide in position 32 of the tRNA anticodon loop determines ability of anticodon UCC to discriminate among glycine codons. *Proc. Natl Acad. Sci. USA*, **90**, 3343–3347.
49. Claesson, C., Lustig, F., Borén, T., Simonsson, C., Barciszewska, M. & Lagerkvist, U. (1995). Glycine codon discrimination and the nucleotide in position 32 of the anticodon loop. *J. Mol. Biol.* **247**, 191–196.
50. O'Conner, M. (1998). tRNA imbalance promotes −1 frameshifting *via* near-cognate decoding. *J. Mol. Biol.* **279**, 727–736.
51. Qian, Q. & Björk, G. R. (1997). Structural alterations far from the anticodon of the tRNA^{Pro}(GGG) of *Salmonella typhimurium* induce +1 frameshifting at the peptidyl-site. *J. Mol. Biol.* **273**, 978–992.
52. Raychaudhuri, S., Niu, L., Conrad, J., Lane, B. G. & Ofengand, J. (1999). Functional effect of deletion and mutation of the *Escherichia coli* ribosomal RNA and tRNA pseudouridine synthase RluA. *J. Biol. Chem.* **271**, 18880–18886.
53. Leung, H. C., Chen, Y. & Winkler, M. E. (1997). Regulation of substrate recognition by the MiaA tRNA prenyltransferase modification enzyme of *Escherichia coli* K-12. *J. Biol. Chem.* **272**, 13073–13083.
54. Davanloo, P., Rosenburg, A. H., Dunn, J. J. & Studier, F. W. (1984). Cloning and Expression of the Gene for Bacteriophage T7 RNA Polymerase. *Proc. Natl Acad. Sci. USA*, **81**, 2035–2039.
55. Nikonowicz, E. P., Sirr, A., Legault, P., Jucker, F. M., Baer, L. M. & Pardi, A. (1992). Preparation of ^{13}C and ^{15}N labelled RNAs for heteronuclear multi-dimensional NMR studies. *Nucl. Acids Res.* **20**, 4507–4513.
56. Batey, R. T., Inada, M., Kujawinski, E., Puglisi, J. D. & Williamson, J. R. (1992). Preparation of isotopically labeled ribonucleotides for multidimensional NMR spectroscopy of RNA. *Nucl. Acids Res.* **20**, 4515–4523.
57. Sambrook, J., Fritsch, E. F. & Maniatis, T. (1989). *Molecular Cloning. A Laboratory Manual*, 2nd edit., Cold Spring Harbor Laboratory Press, Cold Spring Harbor, NY.
58. Legault, P., Farmer, B. T., II, Mueller, L. & Pardi, A. (1994). Through-bond correlation of adenine protons in a ^{13}C-labeled ribozyme. *J. Am. Chem. Soc.* **116**, 2203–2204.

59. Legault, P., Jucker, F. M. & Pardi, A. (1995). Improved measurement of ^{13}C, ^{31}P J coupling constants in isotopically labeled RNA. *FEBS Letters*, **362**, 156–160.
60. Yamazaki, T., Muhandiram, R. & Kay, L. E. (1994). NMR experiments for the measurement of carbon relaxation properties in highly enriched, uniformly ^{13}C, ^{15}N-labeled proteins: application to ^{13}C alpha carbons. *J. Am. Chem. Soc.* **116**, 8266–8278.
61. Altona, C. (1982). Conformational analysis of nucleic acids. Determination of backbone geometry of single-helical RNA and DNA in aqueous solution. *Recueil Rev.* **101**, 413–433.
62. Brünger, A. T. (1992). *X-PLOR Version 3.1 Manual*, Yale University, New Haven, CT.

Edited by D. E. Draper

(Received 21 December 2001; received in revised form 13 April 2002; accepted 16 April 2002)

http://www.academicpress.com/jmb

Supplementary Material comprising five Tables listing ^{1}H, ^{13}C, ^{15}N, and ^{31}P resonance assignments and H1′–H2′ coupling constants is available on IDEAL